Deep Electromagnetic Exploration
K.K. Roy et al (eds)

8. Magnetotelluric Model of Singhbhum Granite Batholith

K.K. Roy, A.K. Singh and C.K. Rao*

Dept. of Geology and Geophysics, IIT Kharagpur, Kharagpur-721 302, India

*Indian Institute of Geomagnetism, Nanabhoy Moos Marg, Mumbai-400 005, India

1. Introduction

A magnetotelluric survey was undertaken across the Singhbhum granite batholith primarily to characterise the electrical structure of the Singhbhum Orissa Iron ore Archaean craton. Metronix MMS02E MT equipment having operating frequency range of 4 Hz to 2.44×10^{-4} Hz was used. Two dimensional model of the subsurface based on one dimensional and two dimensional inversion are presented to show the common features.

1D inversion was done following the approaches of Bachus and Gilbert (1968, 1970), Ridge Regression (Hoerl and Kennard, 1970a, 1970b; Marquardt, 1963; Inman, 1975) Simulated Annealing (Kirkpatrik et al, 1983 and Sen and Stoffa, 1991) and Schmucker's $\rho^* - g^*$ algorithm. 2D inversion was done using the algorithm of Smith and Booker (1991). Electrical model of the subsurface below the Singhbhum granite batholith is presented.

2. Geology of the Area

The Indian subcontinent is subdivided into three proto continents, viz. Singhbhum, Dharwar and Aravalli. These are Archaean and Proterozoic cratons and carry the signature of some of the oldest phases of the crustal evolution. Since the present investigation is restricted to the Singhbhum area only, a brief description of the geology of the area is presented (Saha et al, 1984; Saha et al, 1988; Saha, 1994)

The Singhbhum Orissa iron ore craton (Latitude 20°45′ to 22°45′, Longitude 84°30′ to 86°45′) is bounded to the north and northwest by the 200 km long curved copper belt thrust zone (CBT) and to the south by the Sukinda thrust, which has a nearly east-west strike (Figure 1). The major component of the craton is the Singhbhum granite batholith (8000 km^2). The iron ore craton is surrounded to the east and north east by the relatively high grade Satpura belt and to the south by the Eastern Ghat belt. The oldest rock within the craton is the older metamorphic gneiss (OMG), which consists of medium grade pelitic schists, para and ortho amphibolite and calc schists. OMG covers an area of about 200 km^2 to the west of Champua. These rocks were intruded by biotite, tonalite gneiss grading to

trondhjemite (900 sq km). The rest of the batholith is made up of at least twelve magmatic bodies of biotite granodiorite granite which evolved in two distinct phases (SBGA and SBGB). Recent geochronological studies suggest that SBGA and SBGB are of different age (3.3Ga and 3.1Ga respectively). SBGA rocks are relatively potash poor granodiorite—trondhjemite while SBGB are granodiorite grading to adamellite granite. SBGB occupies nearly two third of the total surface area of the Singhbhum granite batholith (Figure 1). SBGA and SBGB granites have distinctly different physical properties.

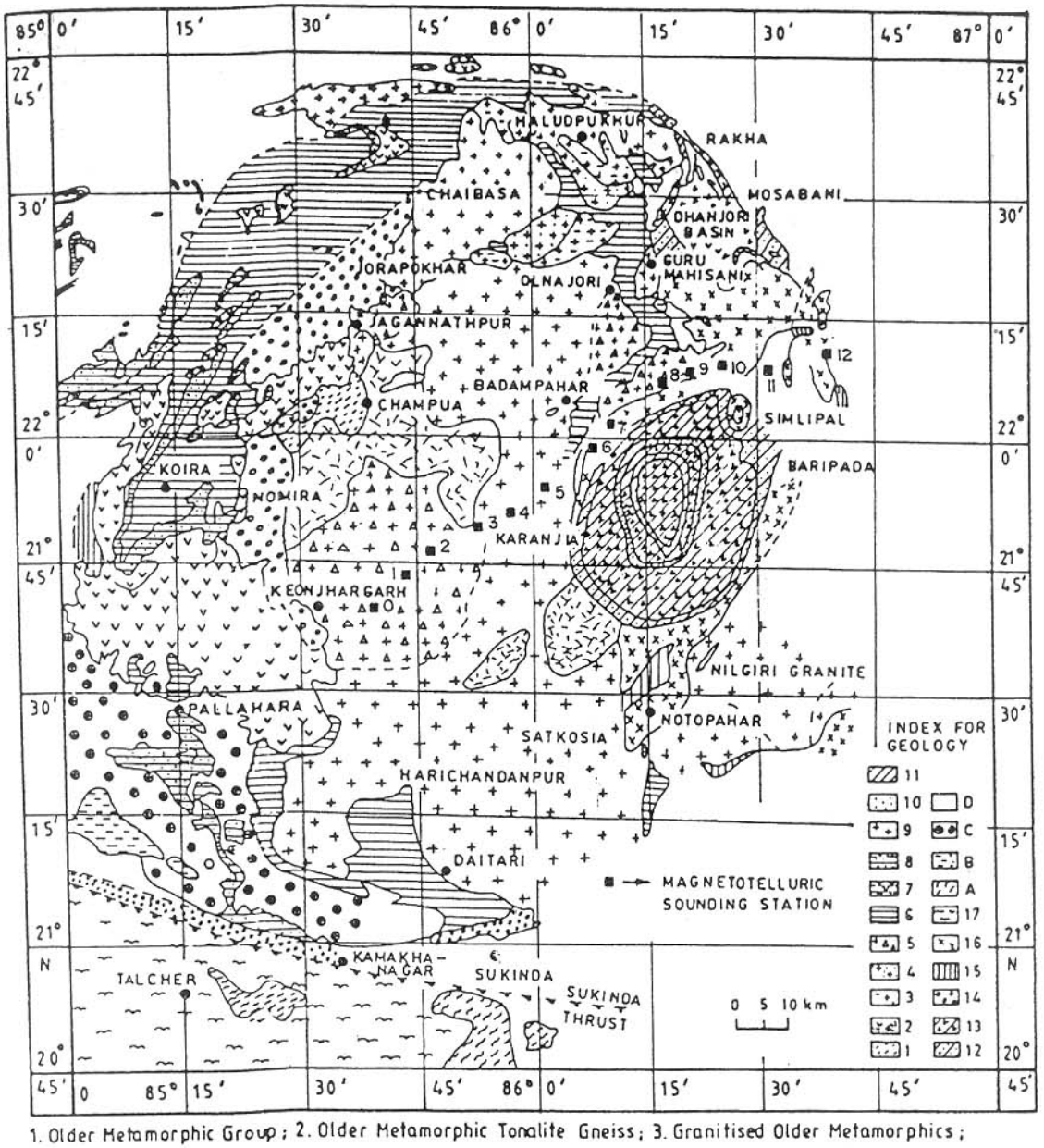

1. Older Metamorphic Group; 2. Older Metamorphic Tonalite Gneiss; 3. Granitised Older Metamorphics; 4. Singhbhum Granite-Phase I; 5. Singhbhum Granite-Phase II; Bonai Granite, Nilgiri Granite; 6. Iron Ore Group; 7. Iron Ore Group Lavas; 8. IOG B.H.J & Quartzites; 9. Sighbhum Granite-Phase III; 10. Singhbhum Group; 11 Dhanjori Group; 12. Dhanjori Group Orthoquartzite; 13. Dhanjori Group Lavas; 14. Kolhan Group; 15. Gabbro-anorthosite; 16. Mayurbhanj Granite; Soda Granite; Arkasani Granite; Chakradharpur Granite; 17. Gondwana; A. Khondalite; B. Charnockite; C. Unclassified Granite-Gneiss; D. Unclassified Rocks

Fig. 1 Geological map of the study area and magnetotelluric observation sites.

Older metamorphic tonalite trondhjemite (OMTG) mineralogically comprises of plagioclase and quartz with accessary biotite and hornblende. They show rather a small range in their chemical composition. OMG and OMTG are about 3.4Ga old and are the oldest group of rocks which form the Singhbhum protocontinent.

3. Field Work

A series of single site magnetotelluric soundings were undertaken across the Singhbhum granite batholith from Bangriposi to Keonjhar. Observation points are shows in Fig. 2. Separation between the field sites ranged between 5 and 15 km. The MMS02E MT system (Metronix, Germany) was used for the field observations and has a frequency range of 4.0 to 1/4096 Hz. Induction coil magnetometer and silver-silver chloride non polarisable electrodes were used for measuring the magnetic and electric fields. Signals up to 628 sec could be retrieved from the overnight continuous observation of 12 to 24 hrs. These signals sense structure upto depth of about 100 km, since they pass through the highly resistive granite batholith. Mono and bivariate choherency threshold of 0.8 was set as the criteria for acceptance or rejection of signals. Rejection of signals due to weak geomagnetic activity was about 60%. North-south and east-west electric field measuring dipole length varied between 60 and 100 meters. Metronix softwares were used for processing of the MT data.

4. Results and Discussion

Figures 3 to 10 are apparent resistivities ($\rho_{a_{xy}}$ and $\rho_{a_{yx}}$) and phases (ϕ_{XY} and ϕ_{YX}) and the 1D inverted models with their uncertainty levels using $\rho^* - g^*$ algorithm of Schmucker for the unrotated and rotated values for the stations Tangavilla, Kadvani, Bubuyajora, Nuvagaon, Dudura, Dari, Badposi and Turumunga. Here northsouth and eastwest components are, respectively, the X and Y components. The apparent resistivities and phases are, respectively, given by

$$\rho_{aXY} = 0.2T \left| \frac{E_X}{H_Y} \right|^2 \tag{1}$$

$$\rho_{aYX} = 0.2T \left| \frac{E_Y}{H_X} \right|^2 \tag{2}$$

$$\phi_{XY} = \tan^{-1} \left| \frac{\mathcal{S}\,|\,E_X/H_Y\,|}{\mathcal{R}\,|\,E_X/H_Y\,|} \right| \tag{3}$$

$$\phi_{YX} = \tan^{-1} \left| \frac{\mathcal{S}\,|\,E_Y/H_X\,|}{\mathcal{R}\,|\,E_Y/H_X\,|} \right| \tag{4}$$

In the dead band (near 1 to 10 Hz) the signals failed to cross the coherency threshold. Therefore, there are some gaps both in the apparent resistivity and phase data.

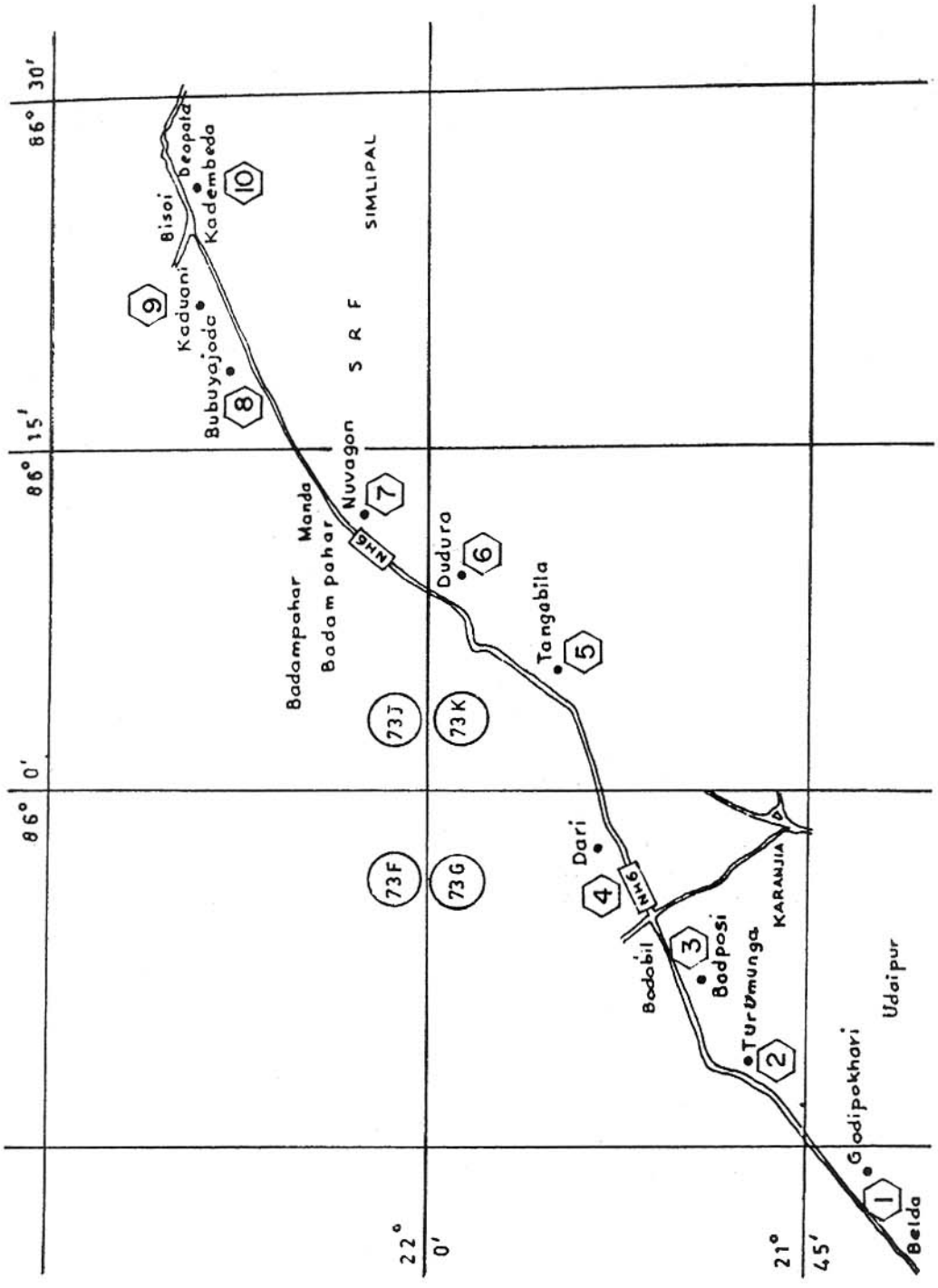

Fig. 2 Location map of the study area and magnetotelluric observation sites.

Four layer earth models are obtained for all the models to show the order of resistivities of the upper crust, lower crust, upper mantle lithosphere, upper mantle asthenosphere.

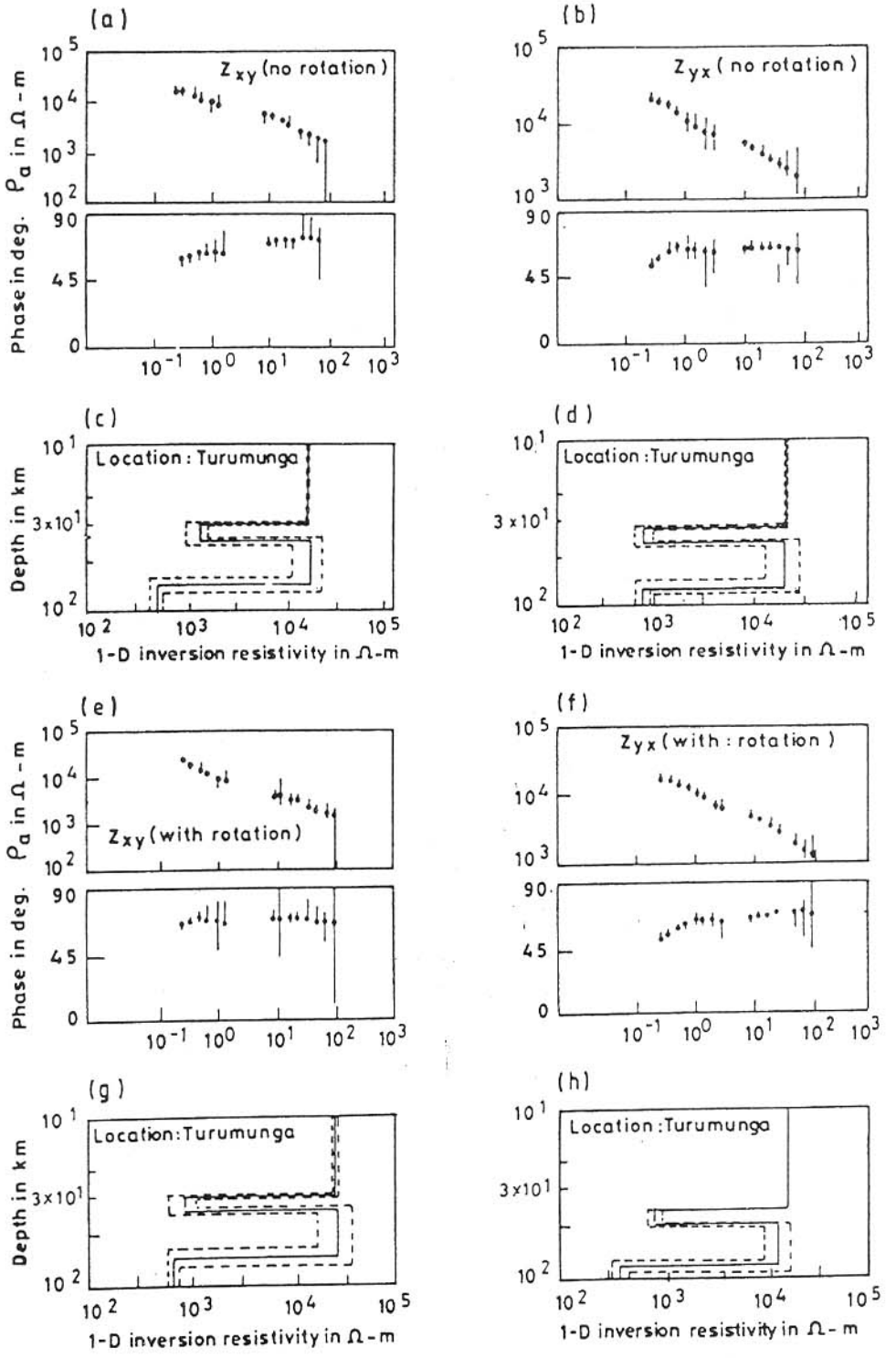

Fig. 3 Magnetotelluric apparent resistivity and phase curves and their inverted section for the Turumunga MT station. a, b shows the unrotated ρ_{aXY} and ρ_{aYX} apparent resistivity and phase field curves and c, d show their 1D inverted sections. e, f shows the rotated ρ_{aXY} and ρ_{aYX} apparent resistivity and phase field curves and g, h show their 1D inverted sections.

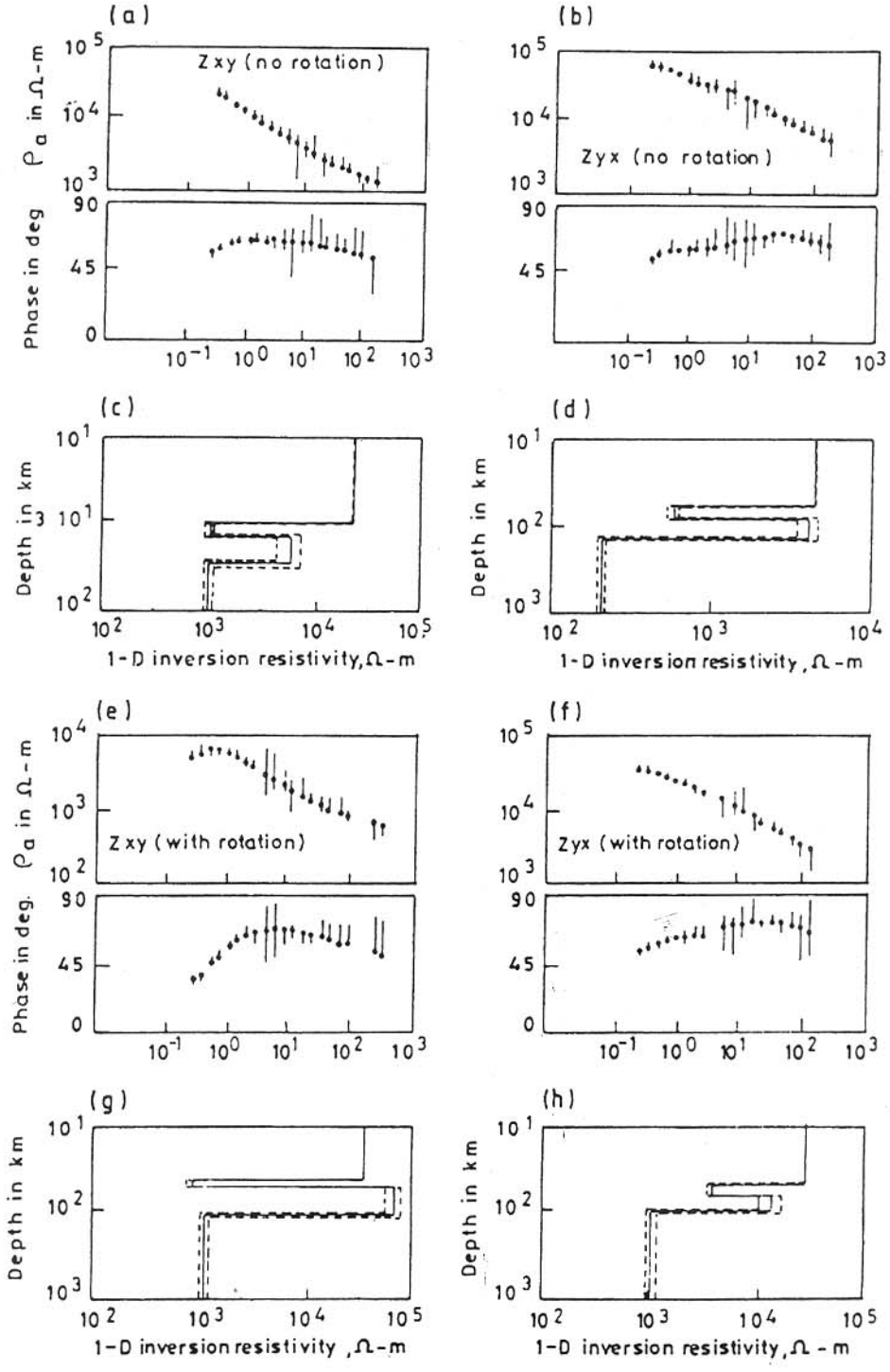

Fig. 4 Magnetotelluric apparent resistivity and phase curves and their inverted section for the Badposi MT station.

Unrotated values are the MT tensors obtained for the geographic north-south and east-west orientation of the electric and magnetic fields. Rotated values are obtained after mathematical rotation of the MT impedance tensors such that at optimum rotation angle, the sum of the squares of the diagonal elements of the tensor

$$\begin{bmatrix} E_X \\ E_Y \end{bmatrix} = \begin{bmatrix} Z_{XX} & Z_{XY} \\ Z_{YX} & Z_{YY} \end{bmatrix} \begin{bmatrix} H_X \\ H_Y \end{bmatrix}$$

i.e., $Z'^2_{XX} + Z'^2_{YY}$ becomes minimum and $Z'^2_{XY} + Z'^2_{YX}$ maximum (Swift, 1969) and is known as Swift rotation angle (Vozoff, 1972). Z′ are the rotated impedance tensors. Eggers (1982) described these rotated and unrotated tensors in detail. Since the trace of the elements of the complex impedance tensors are elliptic and traces of all the elements are of equal size and ellipticity, it is better to work with the maximum value of the impedance

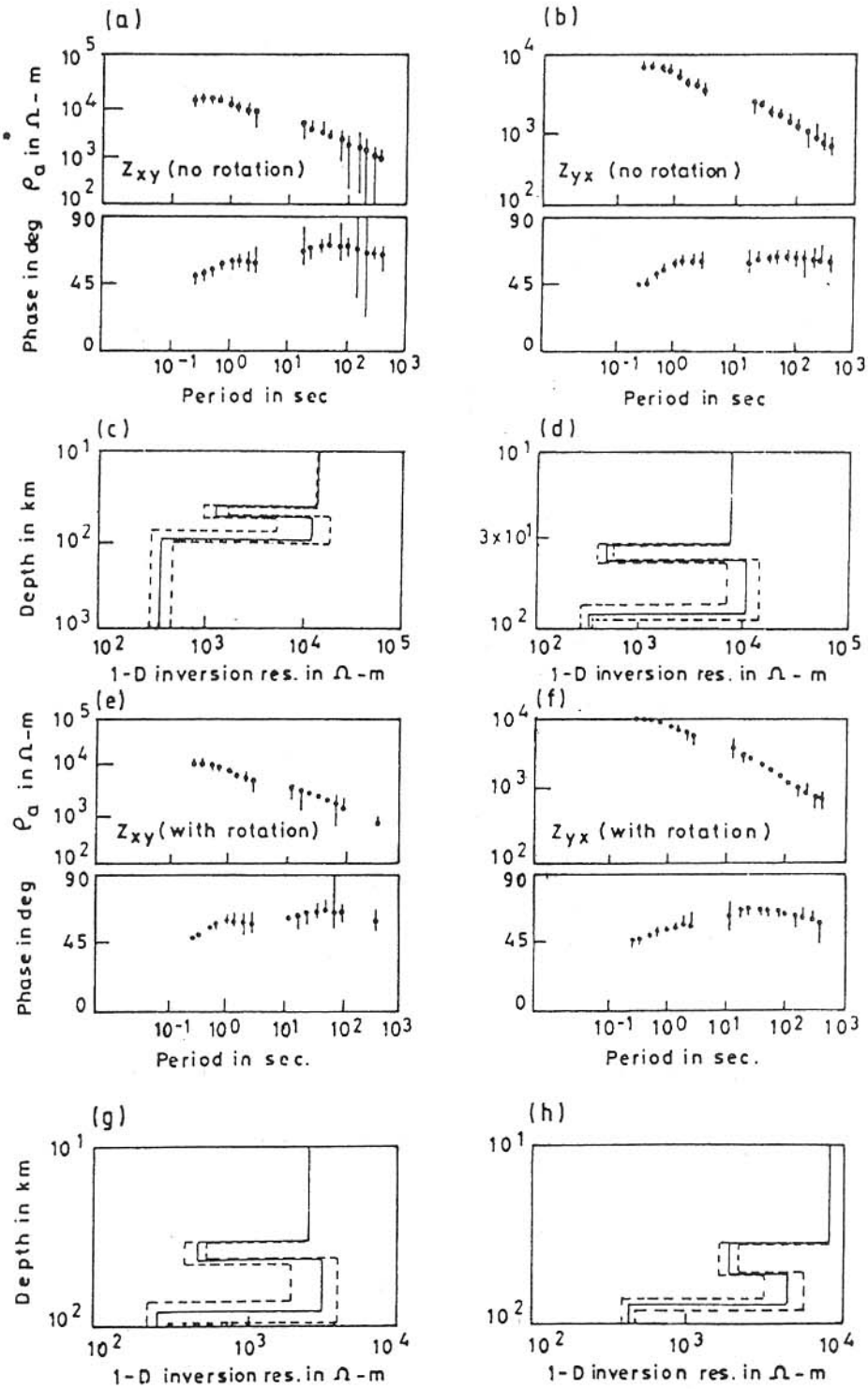

Fig. 5 Magnetotelluric apparent resistivity and phase curves and their inverted section for the Dari MT station.

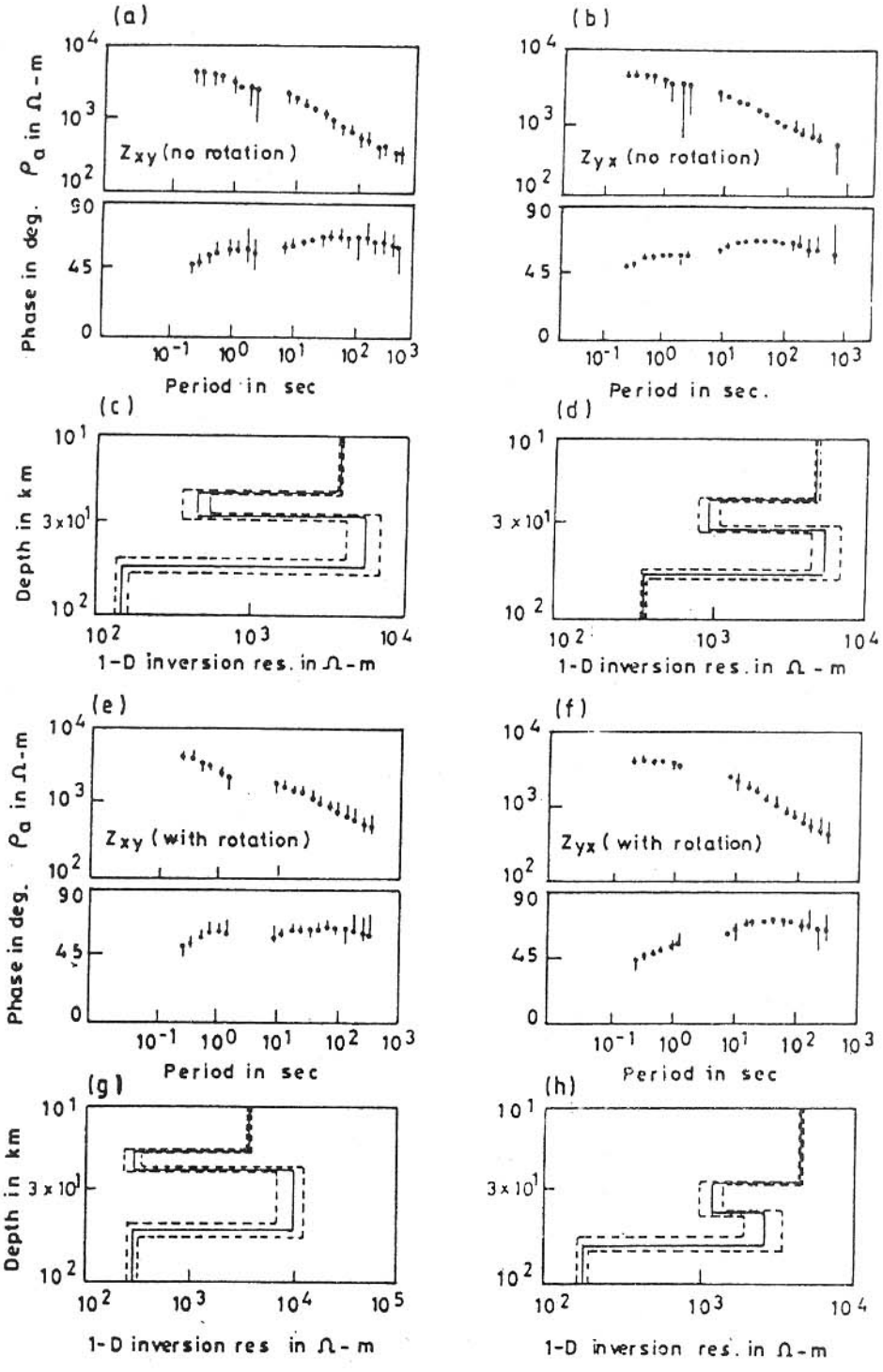

Fig. 6 Magnetotelluric apparent resistivity and phase curves and their inverted section for the Tangavilla MT station.

tensor if we do not go for rotation invariant tensors. That is why optimum rotation is used to have the E and H polarisation values for interpretation. This concept of rotation works nicely for two dimensional problem. For three dimensional earth, this optimum rotation lose its significance to a great extent because $Z'_{XX} + Z'_{YY}$ do not tend towards zero after mathematical rotation.

Figure 11 shows the plots of the Swift Skew

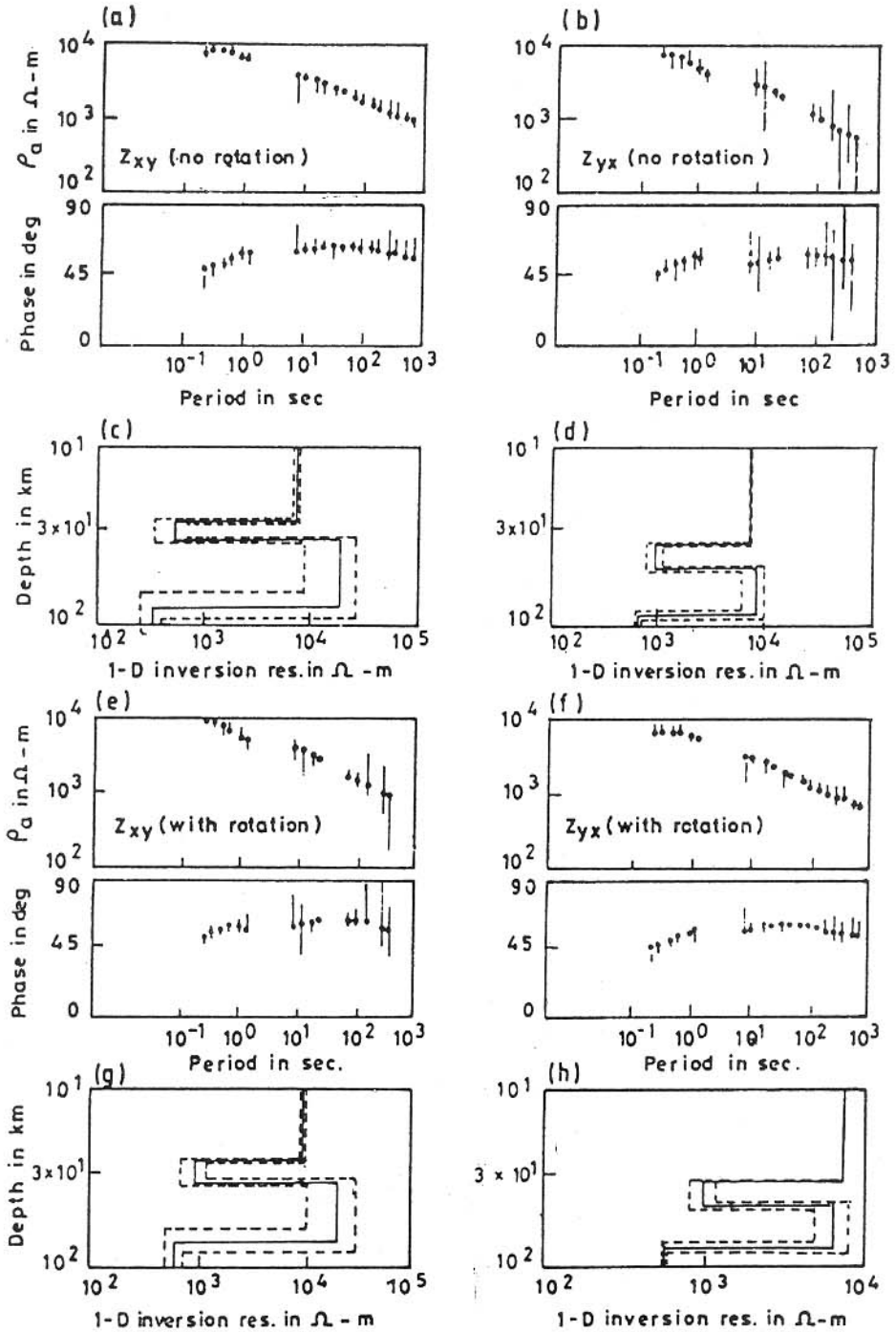

Fig. 7 Magnetotelluric apparent resistivity and phase curves and their inverted sections for the Dudura MT station.

$$\text{Skew} = \left| \frac{Z_{XX} + Z_{YY}}{Z_{XY} - Z_{YX}} \right|$$

for all the frequencies. The Swift Skew plots indicates that the structure is mainly two and three dimensional with several patches of high skews. There are some sites where the skew is low. Along the geological contacts (contacts of SBGA and SBGB, contacts of the Mayurbhanj and Singhbhum granite phase-III i.e., SBGB) skewness plot shows a higher trend. Figures

12 and 13 show the apparent resistivities $\rho_{a_{XY}}$ and $\rho_{a_{YX}}$ plotted along the profile for different periods. At contacts, $\rho_{a_{XY}}$ and $\rho_{a_{YX}}$ separates out. Figure 14 shows the TE apparent resistivity and phase pseudosection. Major contacts are revealed from this figure. Phase pseudosection shows that it is not the case for the static shift.

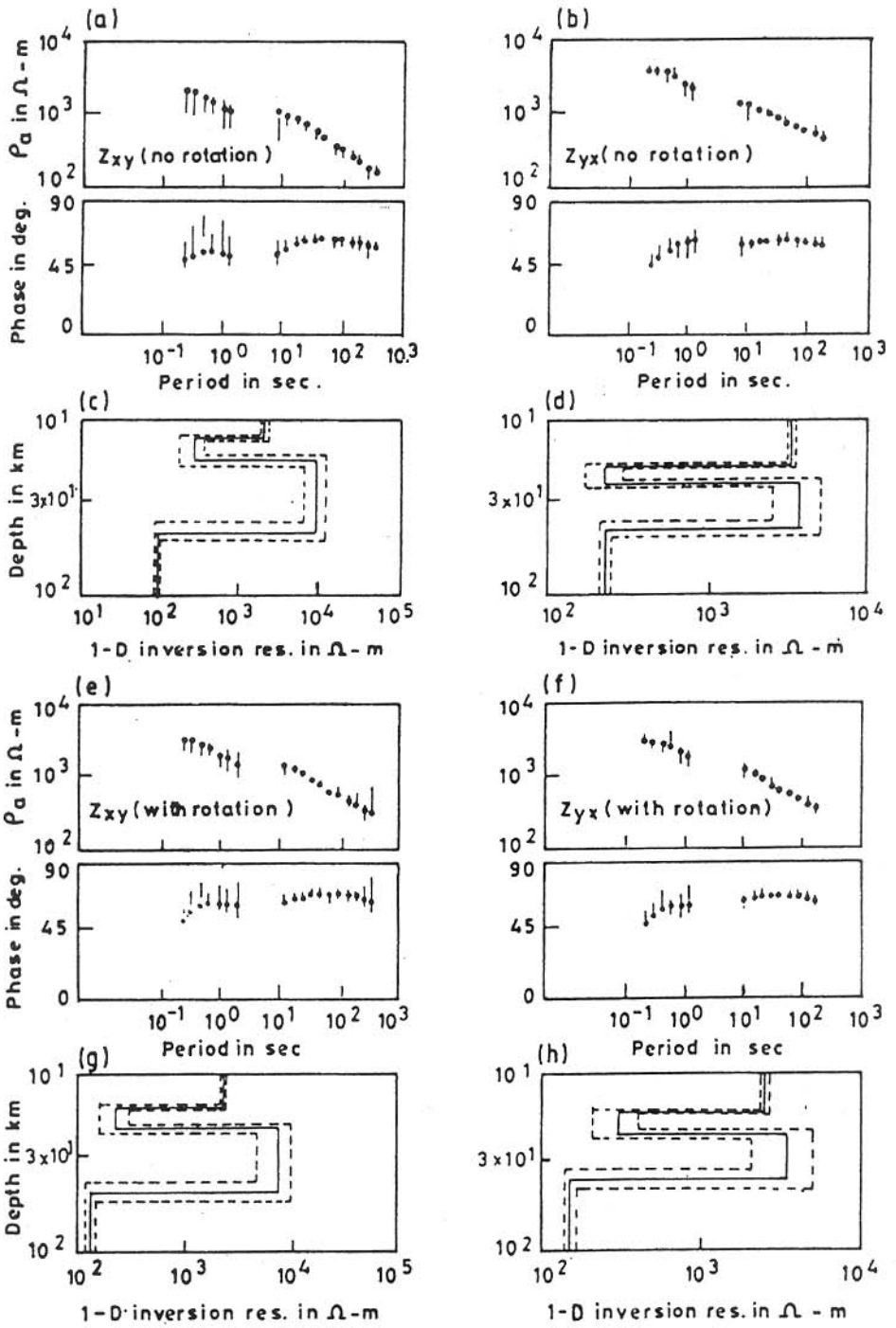

Fig. 8 Magnetotelluric apparent resistivity and phase curves and their inverted sections for the Nuvagaon MT station.

Since the skewness for the Tangavilla station is very low, we tentatively assumed the subsurface structure to be one dimensional. We inverted the TE mode data of this site by Bachus-Gilbert (1968, 1970); Ridge Regression

(Inman, 1975); Simulated Annealing (Kirkpatrik et al, 1983 and Sen and Stoffa, 1991) and Schmucker's $\rho^* - g^*$ algorithm.

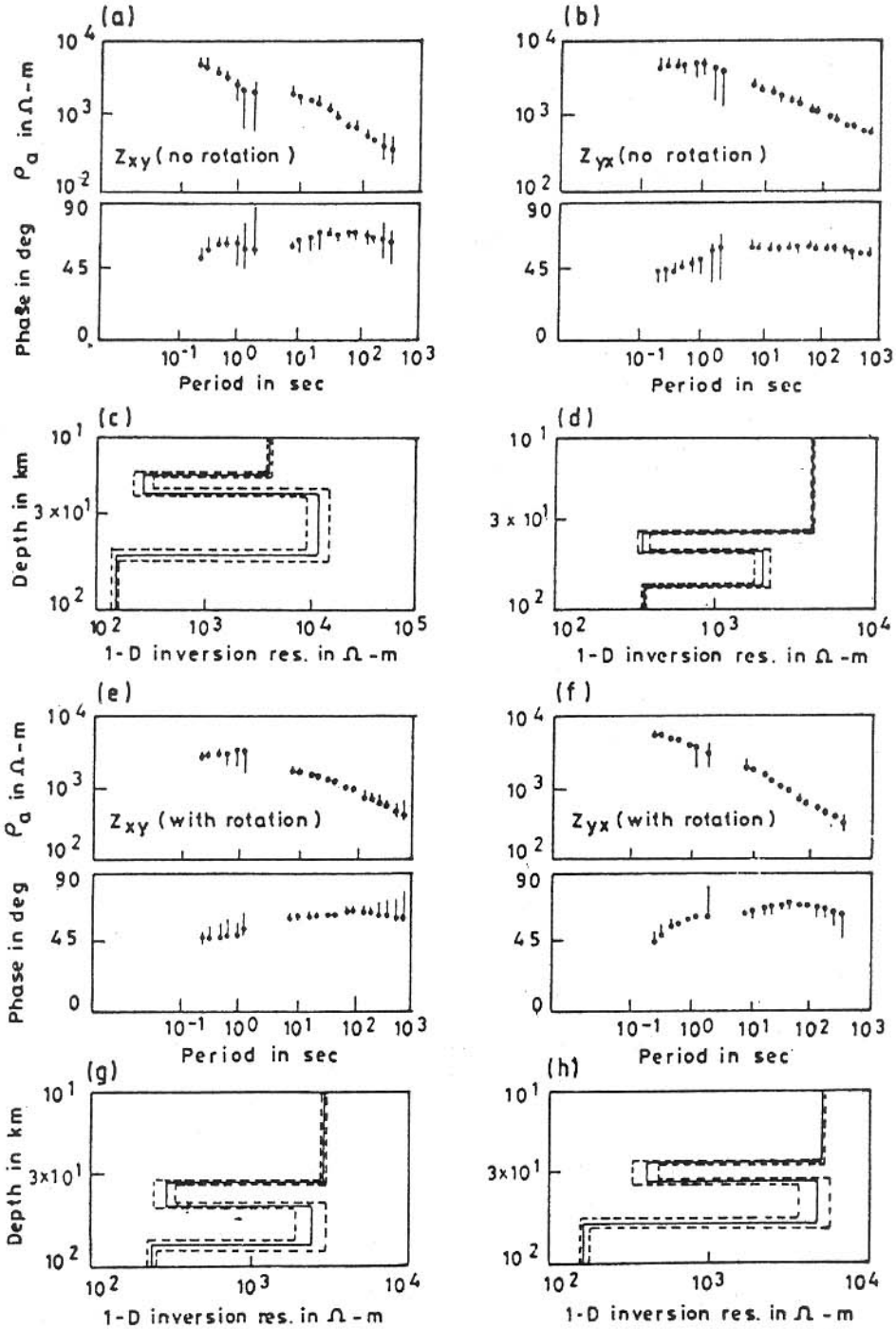

Fig. 9 Magnetotelluric apparent resistivity and phase curves and their inverted sections for the Bubiyajora MT station.

Figures 15 and 16 show the flow charts for the Ridge regression and Bachus-Gilbert inversion. Roy and Routh (1994) have discussed about the procedure adopted for writing the Simulated Annealing algorithm.

Figure 17 shows the apparent resistivity data and initial choice of the model parameters, the Bachus-Gilbert inverted resistivity values, B-G spread function and the B-G averaging kernels for the real field data. Figure 15

shows the depth upto which the MT data could see from the surface. Beyond that depth the B-G spread function starts increasing rapidly. It is also reflected in Fig. 17d which shows how the averaging kernel is losing its deltaness criteria rapidly with depth and it can even be bimodal.

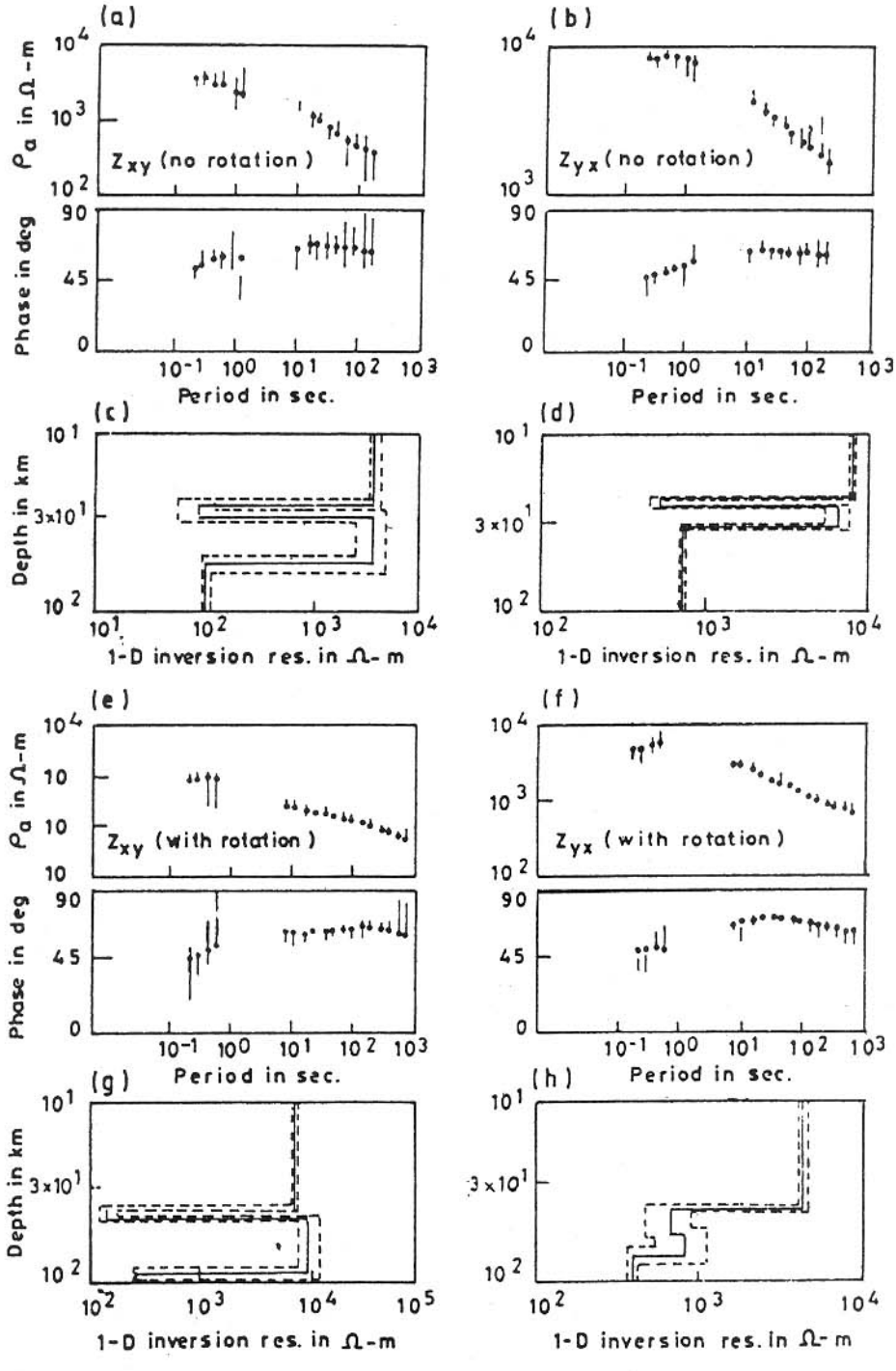

Fig. 10 Magnetotelluric apparent resistivity and phase curves and their inverted sections for the Kadvani MT station.

Figure 18 shows the 1D inverted models obtained by the four different inversion approaches mentioned above. Lower conducting crust is reflected and the depth of the electrical lithosphere boundary at a depth of 60 km and

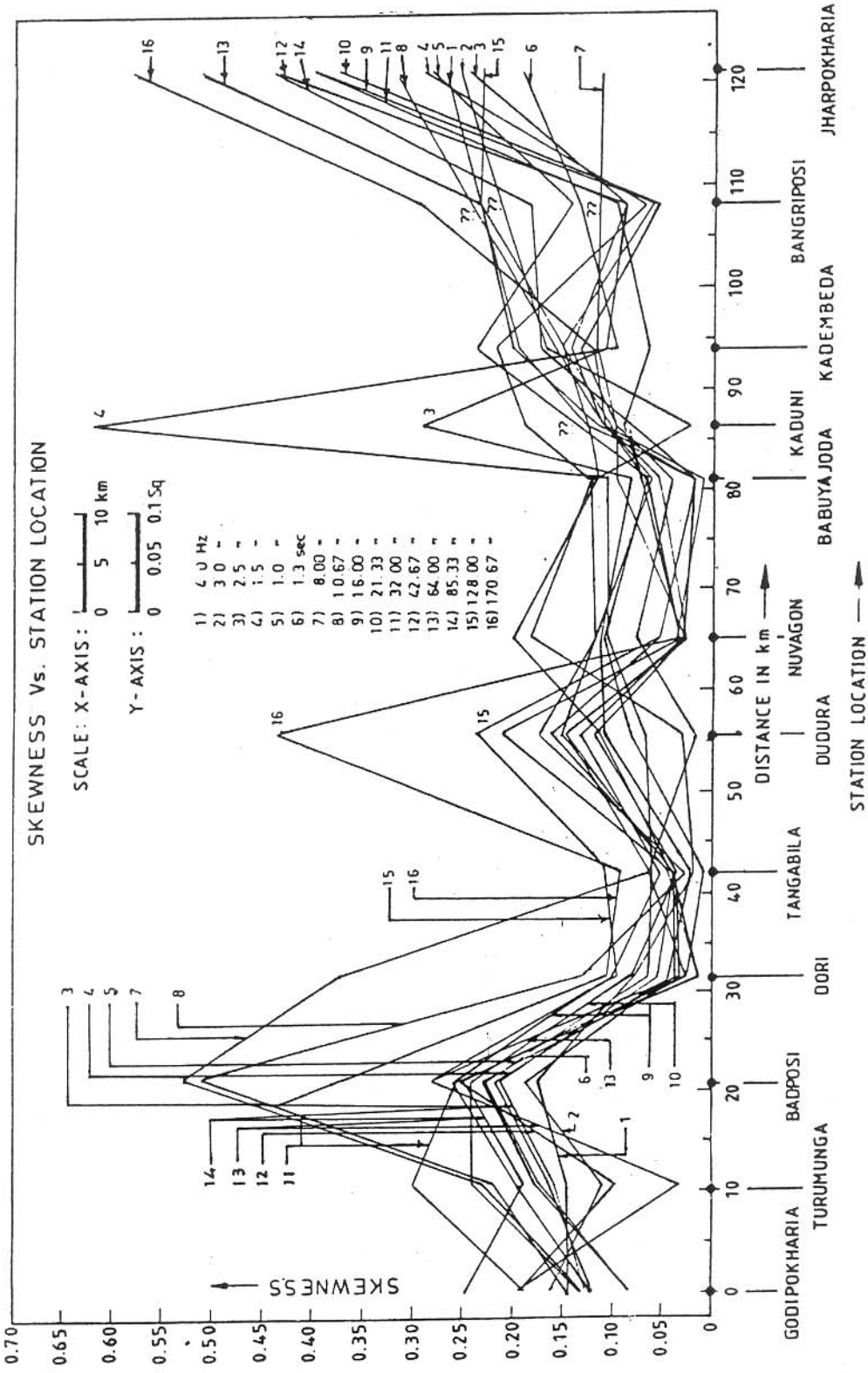

Fig. 11 Nature of variation of Swift Skew along the profile.

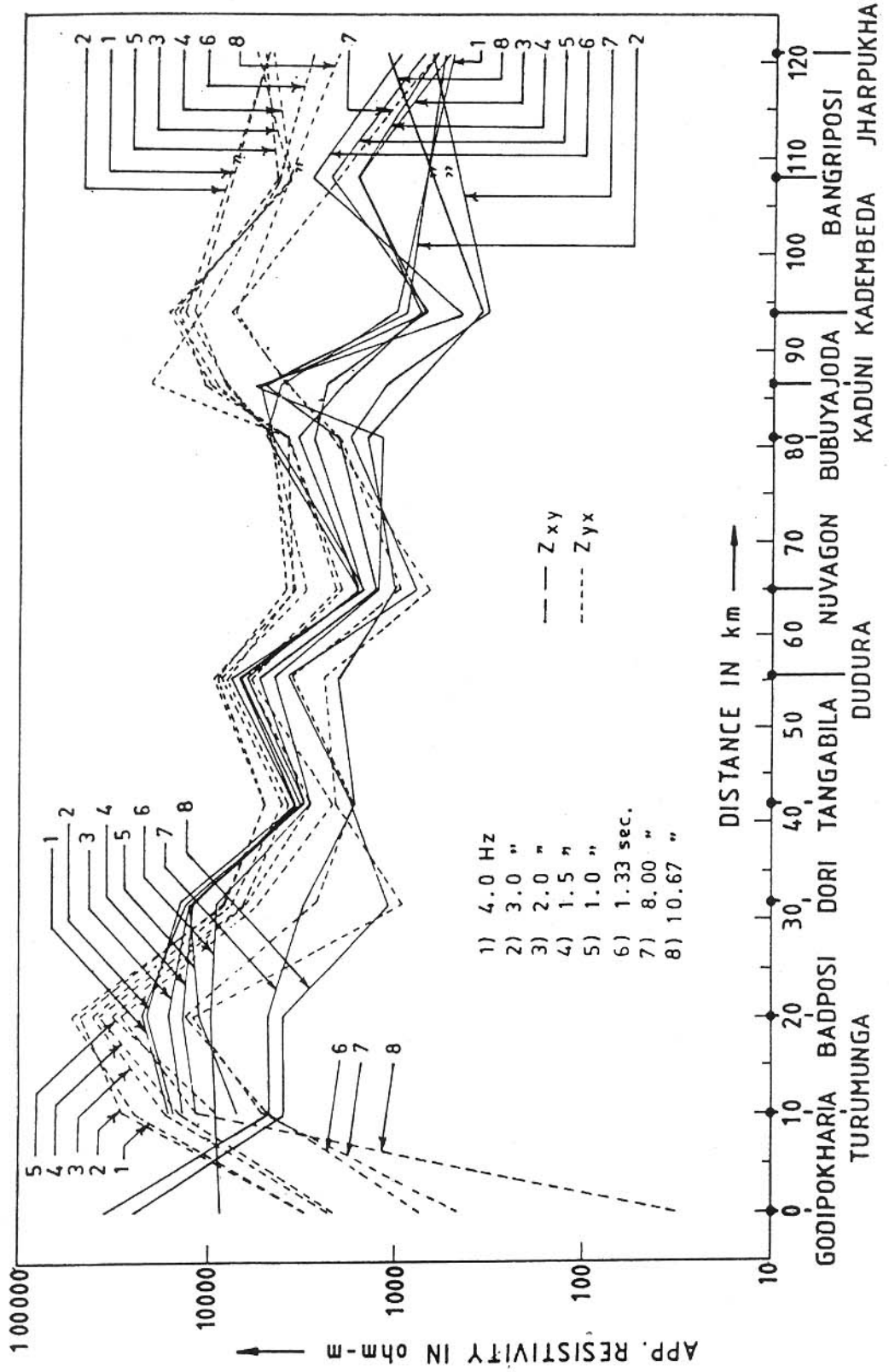

Fig. 12 Behaviour of the apparent resistivities ρ_{aXY} and ρ_{aYX} plotted along the profile for a period from .25 to 10.67 sec.

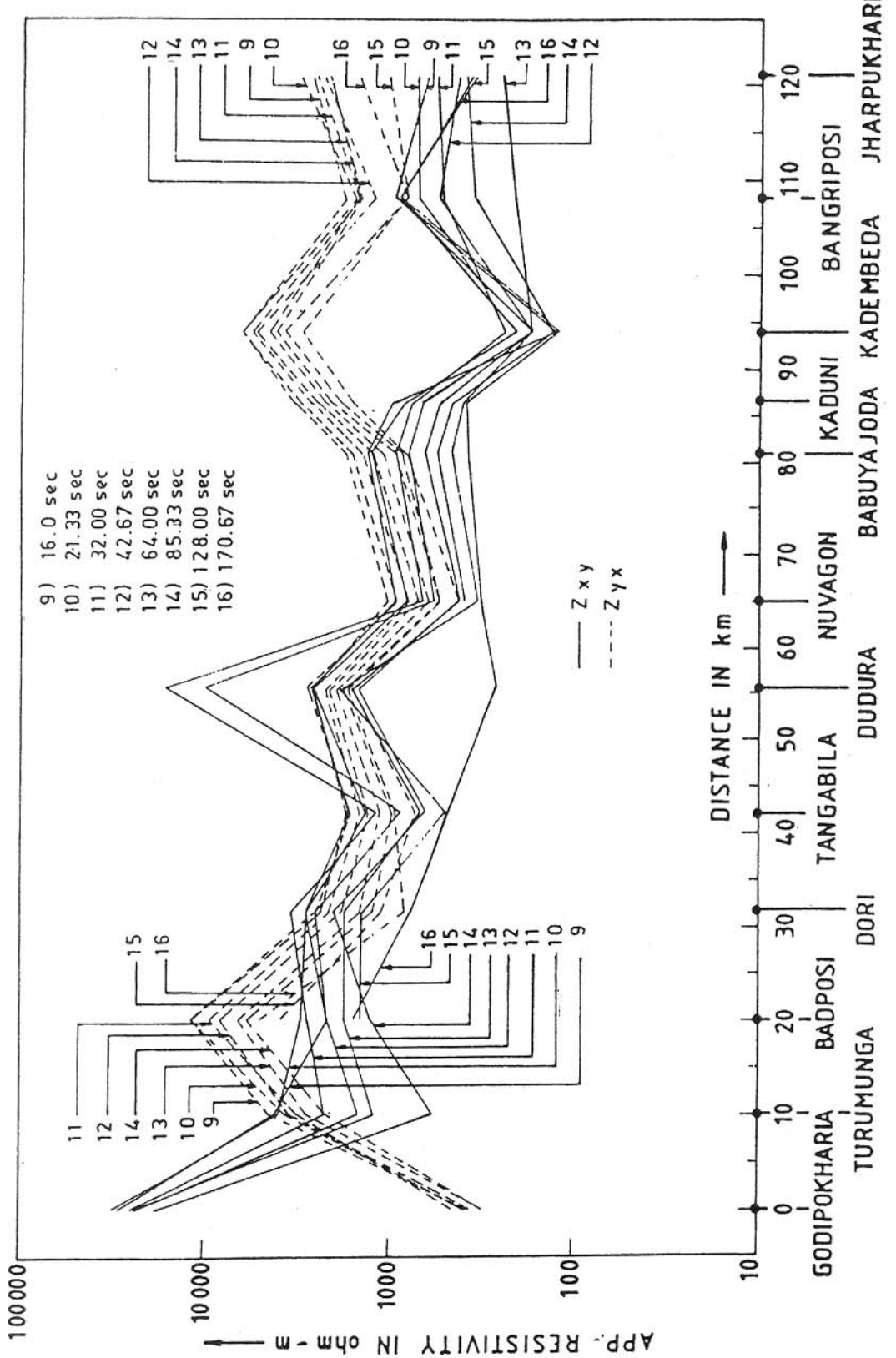

Fig. 13 Behaviour of the apparent resistivities ρ_{aXY} and ρ_{aYX} plotted along the profile for a period from 16.0 to 170.67 sec.

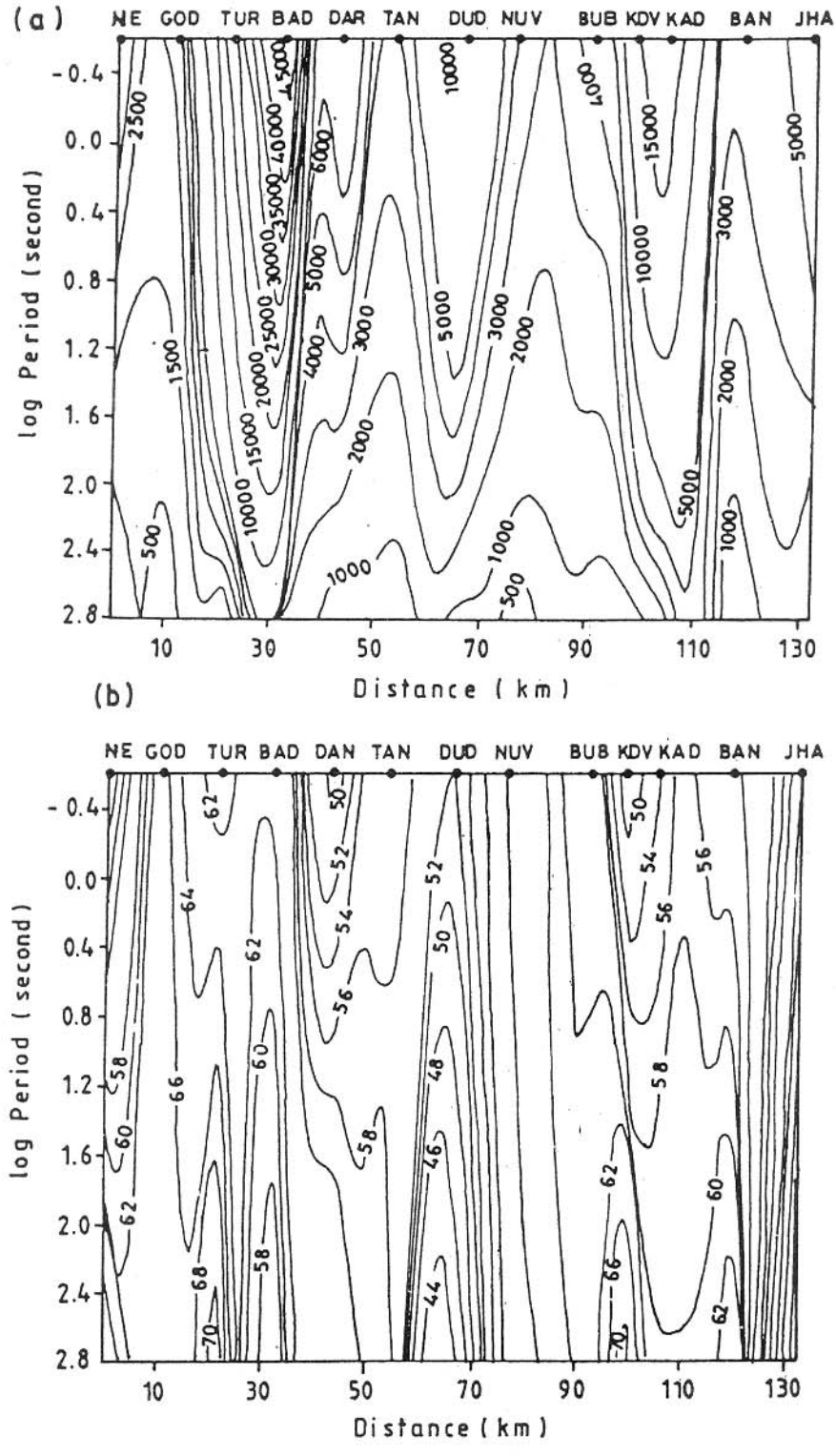

Fig. 14 TE apparent resistivity (a) and phase (b) pseudosection across the Singhbhum granite batholith showing the location of the major geological contacts.

Tangabila MT site. Figure 19 shows the apparent resistivity and apparent phase plots for the sites Tangabila, Badposi, Kadambeda and Bubuyajora. Although the apparent resistivity plots shows a frequency independent vertical shift but the phase curves rules out the case for a static shift (Jones, 1988).

Figure 20 shows the 2D section of the Singhbhum granite batholith based on the 1D inverted data (Model-A). The structure below the Singhbhum granite batholith is broadly a four layer structure. Granite and granodioritic upper crust extends upto 10 to 15 km from the surface. It is underlain by a conducting lower crust of about 10 to 20 km thickness. The upper most mantle (about 25 km thick) lies below the conducting lower crust. Below the upper most mantle lies the conducting asthenosphere.

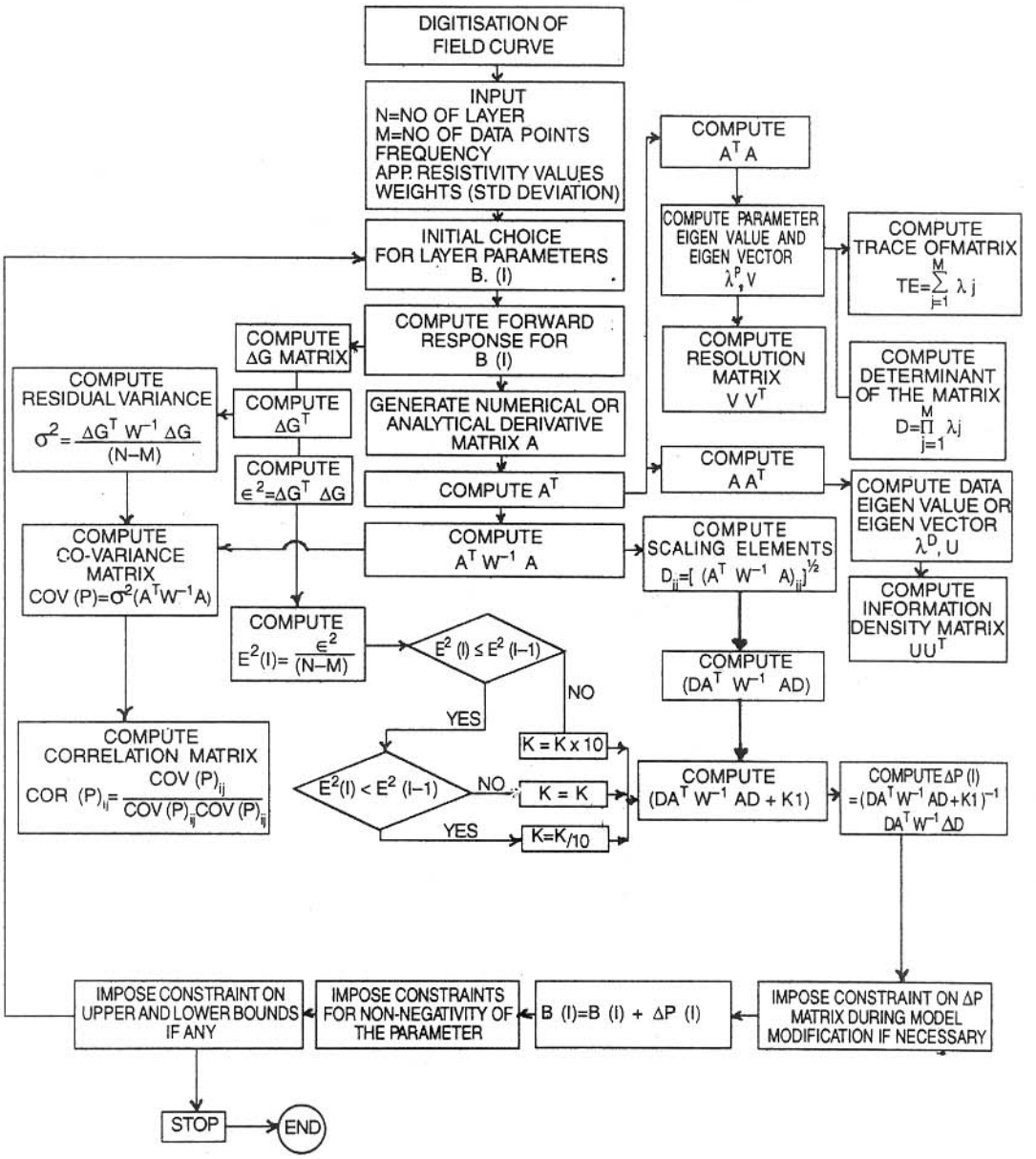

Fig. 15 Flow chart for the weighted ridge regression algorithm.

Park (1983, 1985) mentioned that 1D inverted MT data in the vicinity of the 3D structure will show unusually increase the electrical conductivity of the lower crust. Therefore, these enhanced conductivities may be due to the defects in the artifacts.

"Rapid Relaxation Inversion" (minimum structure algorithm) is used for inverting the TE and TM mode apparent resistivity and phase data. Figure

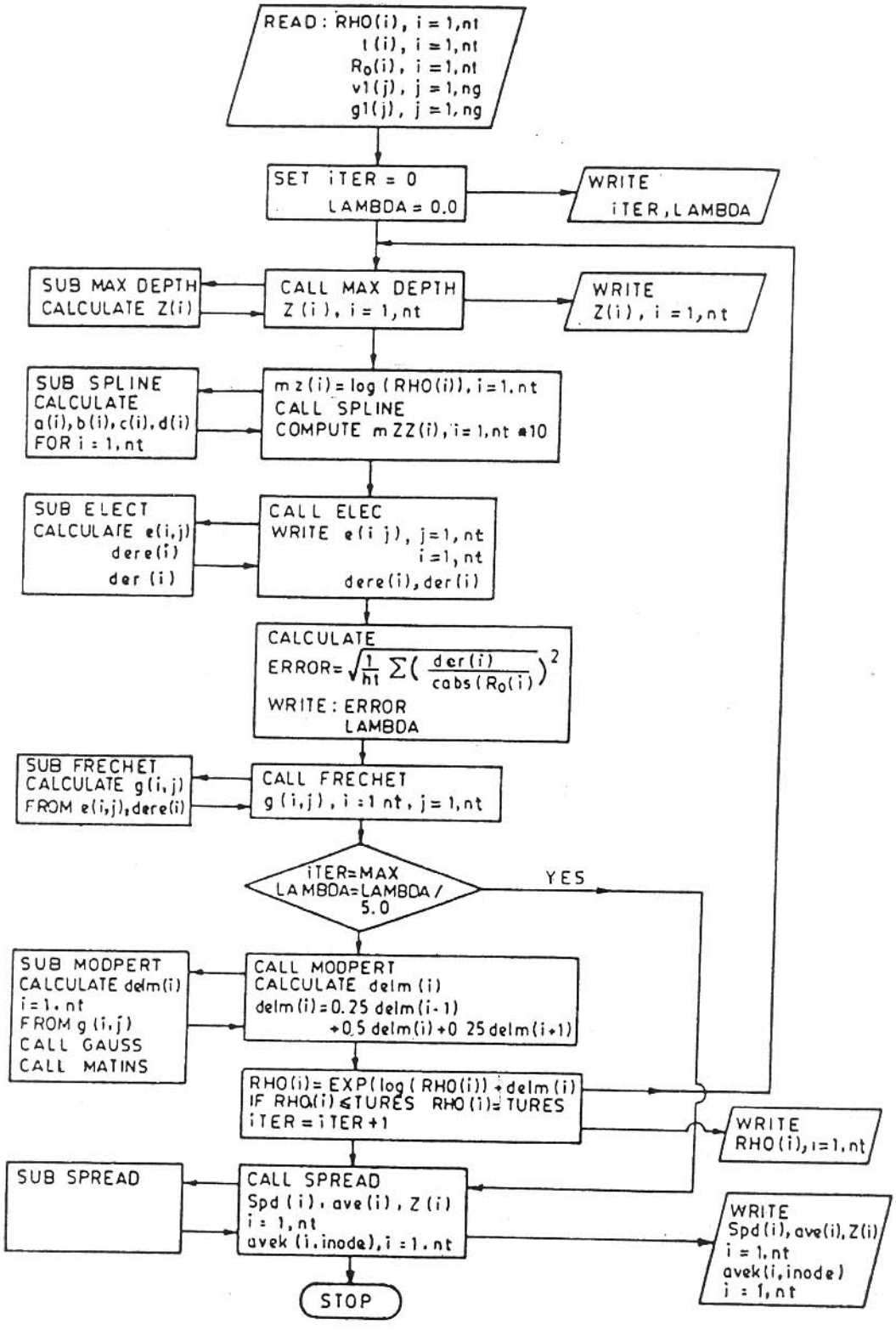

Fig. 16 Flow chart for the Bachus-Gilbert inversion approach.

21 shows 2D inverted models for TE mode (Fig. 21b, c, d), TM (Fig. 21e, f, g) and TEM mode (Fig. 21h, i, j) data. It is observed that all the 2D section for TE, TM and TEM modes are not approximately similar. It indicates that the structure is basically three dimensional.

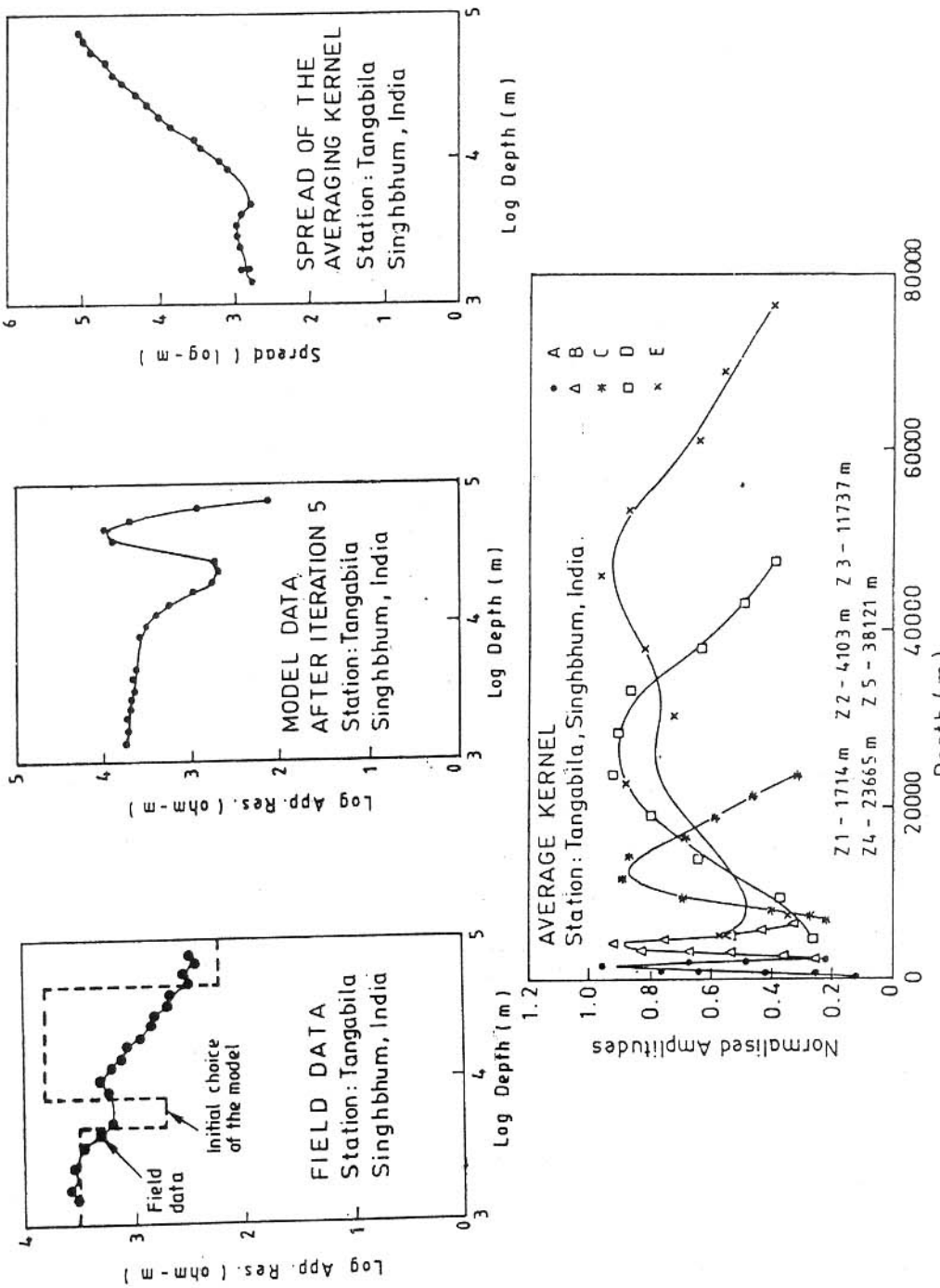

Fig. 17 **B–G inversion results for the station Tangavilla: (a) shows the initial choice of the model, (b) results after inversion, (c) spread of the averaging kernel and (d) shows the averaging kernel.**

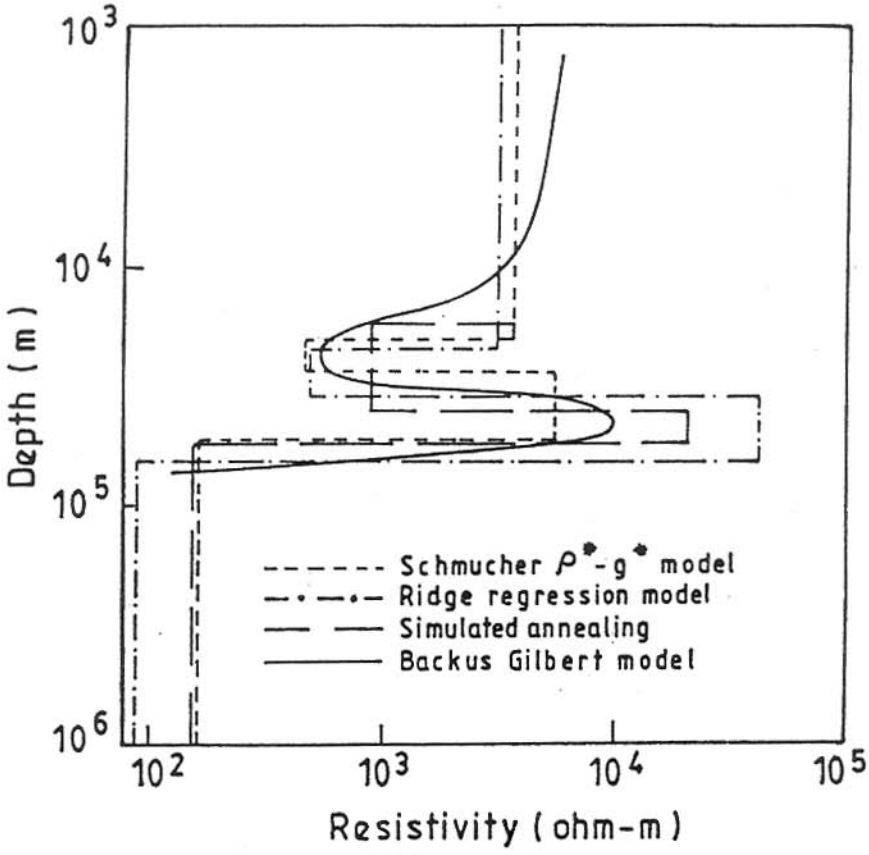

Fig. 18 Resistivity depth section for the Tangavilla MT station using: (i) Schmucker's $\rho^* - \rho^*$ algorithm, (ii) Weighted ridge regression, (iii) Bachus-Gilbert approach and (iv) Simulated annealing.

Figures 20 and 21 reveal following three important features:

1. Thinning of the lithosphere and rising of the mantle material near the station Nuvagaon, which is also there in the section obtained by 1D inversion. Features are sharper in the 2D inverted model.
2. Model-B shows that SBGA i.e., Singhbhum granite phase II (3300 my) is much more resistive and more deep rooted than the SBGB, the Singhbhum granite phase III (3140 my).
3. Lower crustal conductor, which was so prominent is the model-A (Figure 20) appeared only in small patches in model-B (Figure 21)
4. Depth of the electrical lithosphere below Keonjhar is about 80 km in model-A and 130 km in model-B. Depth of the lighosphere below Bangriposi is around 60 km in model A and 70 km in model B. Depth of mantle plume is around 45 to 50 km in both the models.

4.1 Singhbhum Granites SBGA and SBGB

The depth of the Singhbhum granite Phase II (SBG-A) is about 22 km deep and its bulk resistivity is of the order of 18000 Ω-m and above. SBGB is about 3 to 4 km deep covering a large area and its resistivity is of the order of 3500 to 7000 Ω-m.

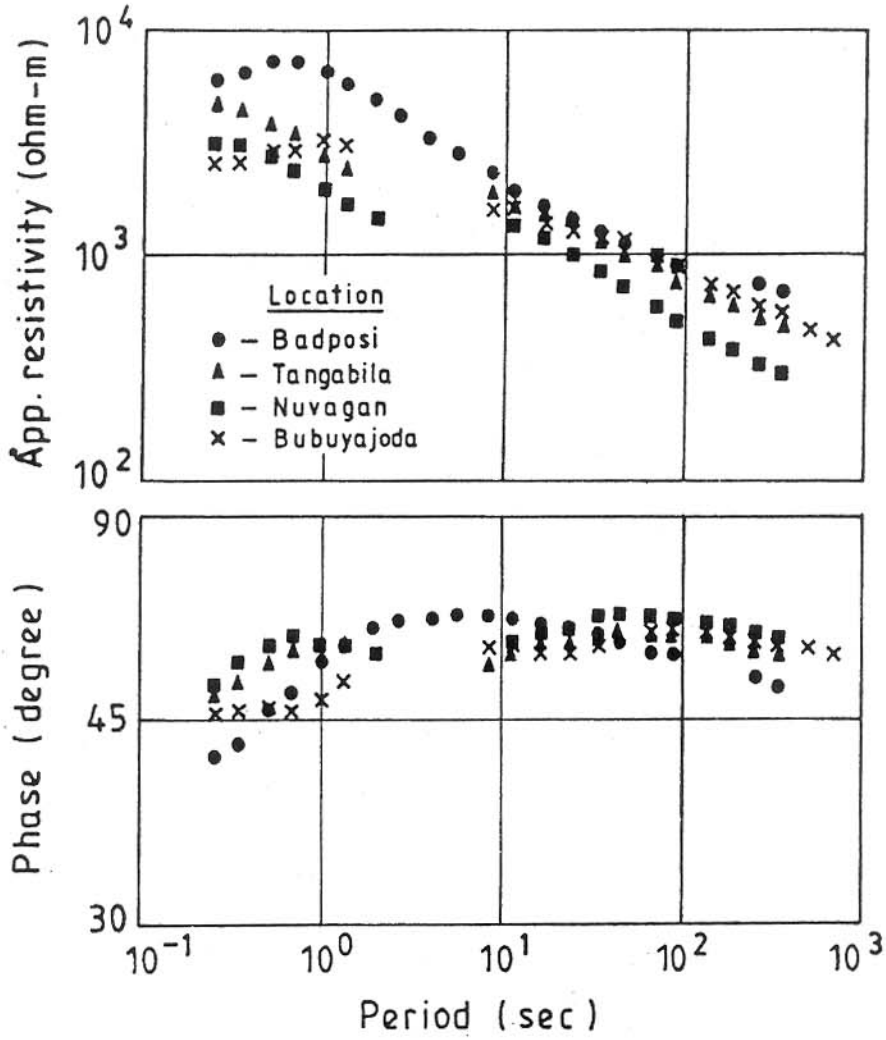

Fig. 19 TE apparent resistivity (a) and phase(b) curves for Tangabila, Badposi, Bubiyajora and Nuvagaon stations.

Thus, from magnetotelluric modelling it appears that SBGA and SBGB are two granite bodies originated from two different parent magma (Saha, 1994). Densities of SBGA and SBGB are, respectively, 2.63 and 2.68 gm/cc (Verma and Mukhopadhyay, 1989). Many geologist believe that SBGA and SBGB actually stand for one granite body. However, geochronology (Bakshi et al, 1987), gravity survey (Verma and Mukhopadhyay, 1989) MT survey and DC resistivity survey (Roy et al, 1993; Roy, 1996) and trace element geochemistry indicates (Saha et al, 1968 and Saha et al, 1984) the existence of two separate granite bodies.

4.2 Mantle Plume

Significant thinning down of the lithosphere and rising of the mantle material below the station Nuvagaon, is apparent both in Model-A and Model-B. Features are sharper in Model-B (Figure 21). It may be a mantle plume. Simlipal volcanics and several dolerite dyke swarms exist very near to this plume type structure. Longitudes of the Dhanjori volcanics, Simlipal volcanics and Sukinda ultramafics are more or less along the same longitude and

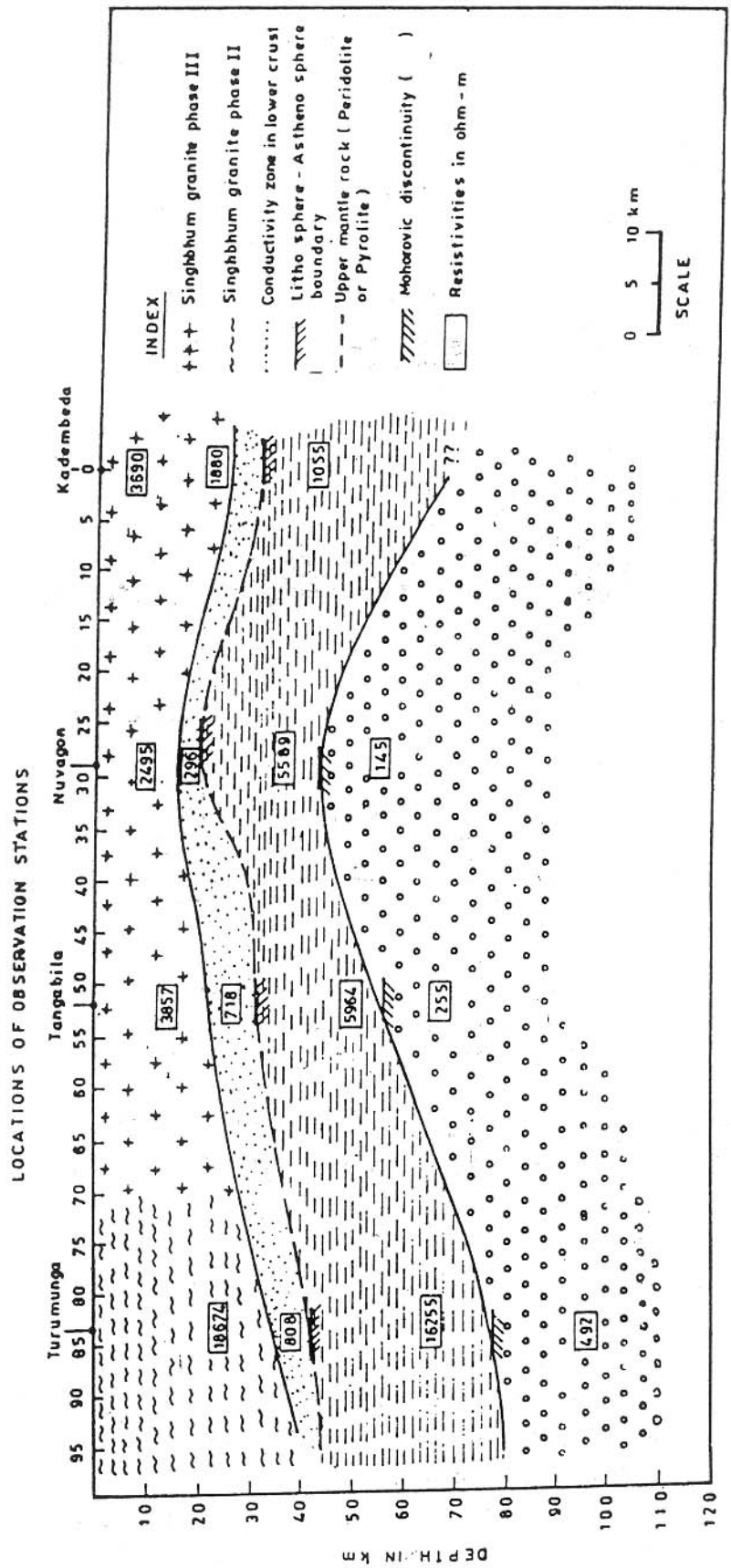

Fig. 20 2D section obtained by 1D inversion and smoothing.

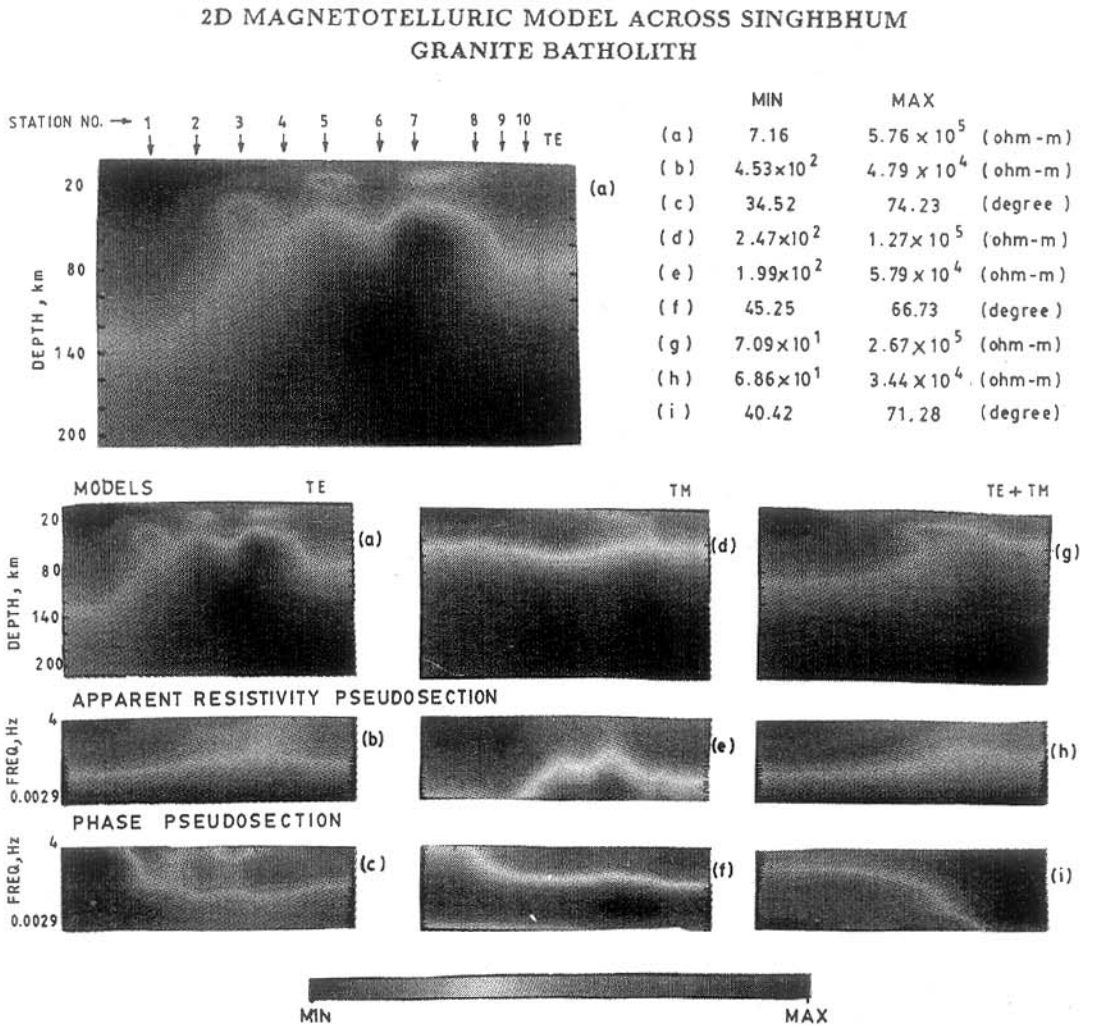

Fig. 21 TE, TM and joint TE and TM mode 2D section and apparent resistivity and phase pseudosections obtained based on 2D rapid relaxation inversion algorithm (RRI) of Smith and Booker (1991).

right above the plume head. Banerjee and Ghosh (1994) have proposed the plume type of structure for Simplipal complex. Their conceptual geological model is roughly matching with the subsurface electrical conductivity model below the Singhbhum granite batholith. Figure 22 shows Bouguer gravity anomaly of the Singhbhum area, prepared by Verma and Mukhopadhyay (1989). It clearly shows the relatively high gravity over Dhanjori, Simplipal volcanics and Sukinda thrust i.e., over the mantle plume.

Possible existence of a mantle plume below the Singhbhum granite batholith is a new concept. Simplipal and Dhanjori volcanics and Sukinda ultramafics are Proterozoic events. It seems the plume existed below the Archaean craton throughout the geological time. To establish this concept, extensive heat flow survey, deep seismic sounding and array type MT survey for 3D modelling and inversion should start. Elevation difference between the plume head and base of the lithosphere should be studied in

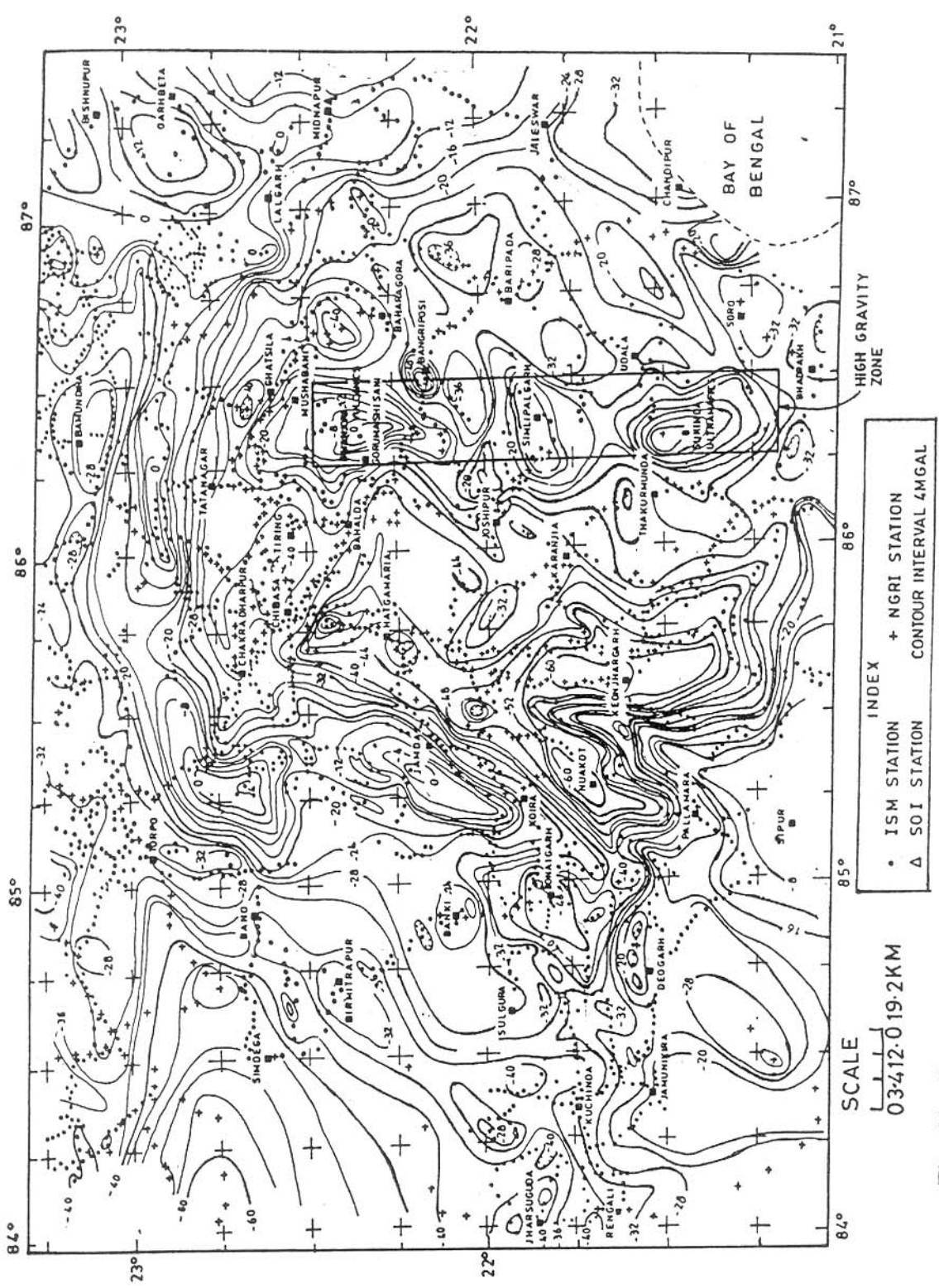

Fig. 22 Bouguer gravity anomaly map of Singhbhum and adjoining area (after Verma and Mukhopadhyay, 1989).

perspective of the isostatic compensation over the geological time period. Since the geological and geophysical work converged towards the mantle plume issue. This problem must be given further attention.

4.3 Asthenospheric Temperature from MT

An attempt was made to estimate the temperature of the asthenosphere approximately based on the available high pressure temperatue experimental electrical conductivity data. High pressure and temperature electrical conductivity data for the crust mantle silicates are taken from the following papers· Bradley et al. (1964), Chanishvilli et al. (1982), Constable and Duba (1990), Constable et al. (1992), Duba et al. (1973) Duba et al. (1974), Duba (1976), Duba and Shankland (1982), Shankland (1982), Duba and Nicholls (1973), Dvorak (1973), Kobayashi and Maruyama (1971), Kariya and Shankland (1983), Lastovickova (1975), Lastovickova and Kropacek (1978), Lastovickova (1979), Lastovickova (1981), Lastovickova et al. (1987), Mackwell and Kohlstedt (1990), Olthoeft (1977), Omura et al. (1989), Rai and Manghnani (1978), Schock et al. (1989), Shankland and Duba (1987), Shankland and Duba (1990), Tyburczy and Roberts (1990).

Figure 23 shows a compilation of the electrical conductivity of different crust mantle silicates at different temperatures. This diagram is based on the published results. We have assumed garnet peridotite as possible composition (as an approximation) of the mantle at the asthenospheric depth. The most abundant mantle xenoliths reported from all over the world are spinel lherzolite (Nixon, 1987). Only Rai and Manghnani (1978) reported some electrical conductivity data on garnet and spinel lherzolite. A thorough study on the electrical conductivity of spinel/plagioclase/garnet lherzolite should start. In an olivine-orthopyroxene-clinopyroxene triangle, lherzolite and peridotite have major overlapping areas. Therefore their electrical conductivities may or may not be different. Since electrical conductivity follows a different path while heating and cooling (Lastovickova, 1983) and samples of crust mantle silicates collected from different parts of the world show different electrical conductivity, therefore the electrical conductivity of a particular silicate vary over a wide range at a particular temperature. Figure 23 shows the range of resistivities of the crust mantle silicates. The electrical conductivities, of the samples studied, extend over a several order of magnitude at a particular temperature. As a result the estimated temperature of the asthenosphere was within the range 1000 to 1400°C. With more information of high pressure temperature electrical conductivity of the crust—mantle silicates and 3D inverted conductivities from MT survey, this kind of exercise can be made more accurate and meaningful in future.

4.4 Lithospheric Thickness

Lithospheric thickness has become a debatable issue. Magnetotelluric method

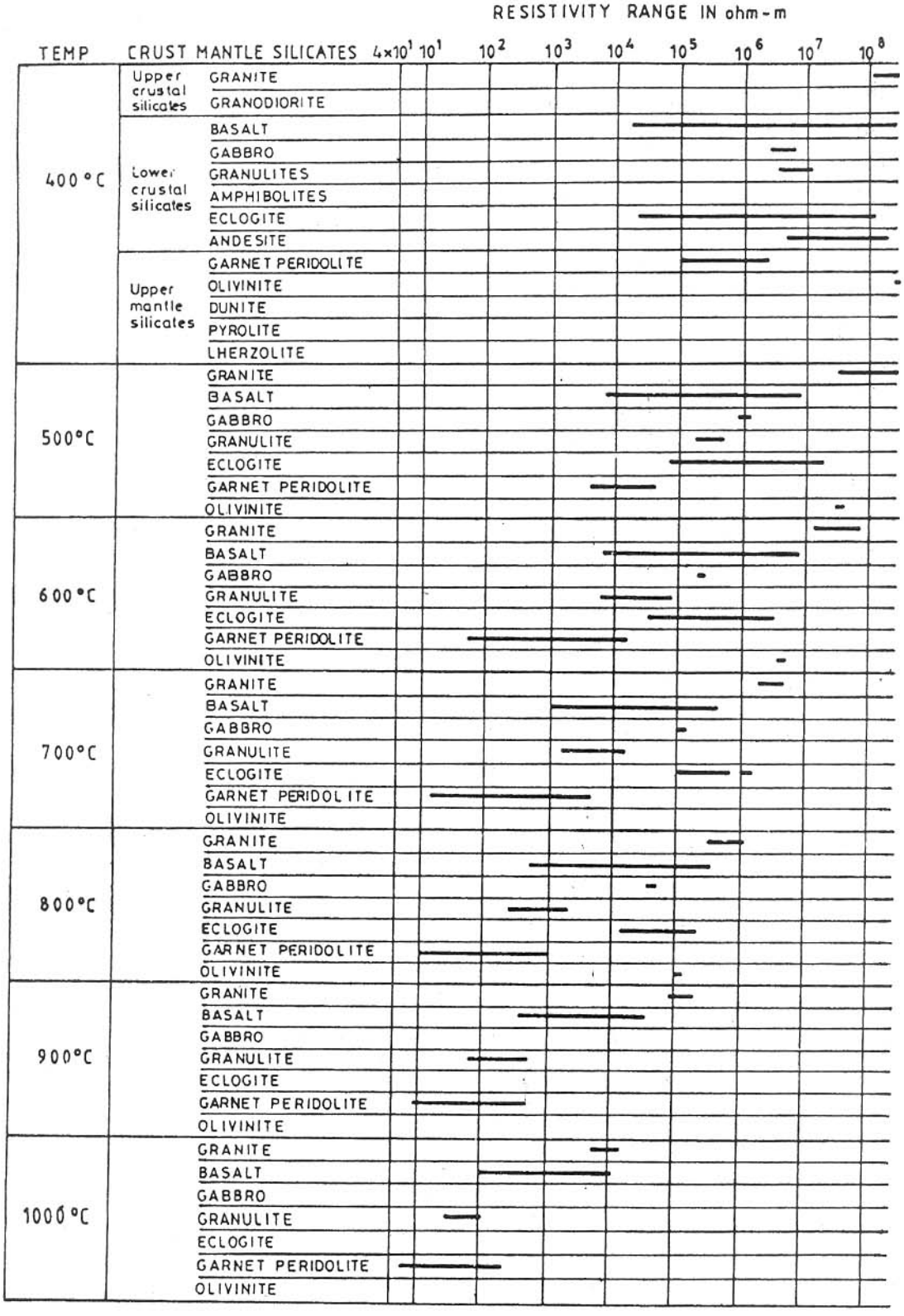

Fig. 23 High pressure temperature experimental data.

certainly is a powerful tool for determining the thickness of the electrical lithosphere. But none can be sure whether he has measured the depth of the lithosphere. Because seismic, thermal, chemical, petrological, seismic and electrical lithospheres exists in the literature and the depths of the boundaries are not same. The general idea surrounds the following points: (a) as the

LA boundary should be a brittle-ductile transition boundary, this is the depth where a sharp change in the rheological property should exist; (b) this is the depth where low velocity zone starts and (c) this is the upper limit of the whole mantle or upper mantle convection cells. The fact is, if the hardness of the mantle rock suddenly changes at a particular depth then seismic velocity (P and S) and electrical conductivity should also change significantly. In reality the reported estimates of the lithospheric thickness by magnetotellurics are lower than that obtained by seismics. What can be the possible answer?

If the discrepancy between the seismic and electrical lithospheric depth is very large then the sudden rise in the electrical conductivity at a depth of around 50 to 150 km in the absence of the seismic signature may be due to some reasons other than change in the rheological properties. The authors are proposing mantle metasomatism as on of the reasons for enhanced electrical conductivity at a depth of 50 to 150 km. Hydrous minerals like serpentine, epidote, phlogopite, dolomite, amphibole can originate due to the reaction of the mantle volatiles with the silicates. Serpentinisation may be the most probable cause. The following chemical changes can occur in the upper mantle depth (Fyfe, 1981).

$$\underset{\text{Water}}{2H_2O} + \underset{\text{Pyroxene}}{MgSiO_3} + \underset{\text{Olivine}}{Mg_2SiO_4} \rightarrow \underset{\text{Serpentine}}{Mg_3Si_2O_5(OH)_4}$$

$$\underset{\text{Pyroxene}}{6MgSiO_3} + \underset{\text{Water}}{3H_2O} \rightarrow \underset{\text{Talc}}{Mg_3Si_4O_{10}(OH)_2} + \underset{\text{Serpentine}}{Mg_3Si_2O_5(OH)_4}$$

$$\underset{\text{Forsterite}}{2Mg_2SiO_4} \rightarrow \underset{\text{Serpentine}}{Mg_3Si_2O_5(OH)_4} + \underset{\text{Brucite}}{Mg(OH)_2}$$

$$\underset{\text{Olivine}}{Mg_2SiO_4} + \underset{\text{Pyroxene}}{MgSiO_3} \rightarrow \underset{\text{Serpentine}}{Mg_3Si_2O_5(OH)_4}$$

The authors propose that serpentinisation or accumulation of other hydrous minerals can increase the electrical conductivity where seismic velocities may not have any significant variations. In other words, the depth of the electrical and seismic lithosphere may or may not be the same. Reported lithospheric thicknesses based on magnetotelluric survey are on the lower side in comparison to that obtained by seismic methods on an average. The lithospheric thickness obtained in this study varies from 130 to 60 km. Pollack and Chapman (1977), based on the global distribution of heat flow data, has prepared the lithospheric map of the world. In that the thickness of the Indian lithosphere is shown to be below 100 Km. Lithospheric thickness obtained by other organisations in India from magnetotelluric studies are of the order of 100 to 120 Km (Gokern et al, 1992).

Thickness of the lithosphere in the Singhbhum craton approximately varied from 130 to 50 km.

Pollack and Chapman (1977) prepared the global heat flow and lithospheric map on the basis of the 12° harmonic plot of the heat flow data. They have

shown that the heat flow near the Singhbhum craton to be 60 mWm^{-2} and the lithospheric thickness is 75 km. One available heat flow result from the copper belt thrust zone of the Singhbhum, is 54.5 ± 5 mWm^{-2} (Shankar, 1988). Anderson (1995) hinted at the chemical enrichment and metasomatism within upper mantle as the probable cause of enhanced electrical conductivity without bringing in the appreciable changes in seismic velocities.

It is an important question to be answered in future. If Lithosphere and Asthenosphere boundary is a boundary of brittle-ductile transition, if viscosity of the brittle lithosphere is 2 to 3 order of magnitude higher (Anderson, 1995) than that of the asthenosphere then both seismic velocities (V_P and V_S) and electrical conductivity should change sharply. In other words estimated lithospheric thickness by MT and deep seismic sounding should be closer. In reality if the two estimates differ widely, then what can be the possible reasons. It is due to

1. 1D interpretation of 3D MT data.
2. Poor data quality.
3. Chemical enriched relatively shallower portion of the lithospheric upper mantle becomes too conductive to allow MT signals with reasonable resolving power to go further down to detect the lithosphere—asthenosphere boundary. This chemical enrichment may be due to serpentinisation, presence of continuous phase of graphite and mantle fluids H_2O-CO_2-S.

4.5 Lower Crustal Conductor

Although 1D interpretation by four different approaches show the presence of the lower crustal conductor, 2D model obtained by Smith and Booker (1991) RRI approach did not show the lower crustal conductor as a prominent feature. It is present in patches at three places.

Wyllie (1988), Fyfe (1986), Fyfe (1988), Haak and Hutton (1986), Shankland and Anders (1983), Hyndeman and Hyndeman (1968), Hyndeman and Shearer (1989) have discussed on the possibility of having fluids in the lower crust. Besides meteoric water which percolates down to 15 km from the surface, fluids from within the earth's mantle are continuously moving upward as volatiles. These H_2O-CO_2-CH_4-S volatiles can generate significant amount of fluids to form a continuous phase. At lower crustal depth the temperature is generally of the order of 400° to 500°C with a pressure range of 8 to 10 Kb. Unless there is strong underplating and accretion in the crust by mantle plumes, the environment is suitable for green schist facies to amphibolite facies metamorphism. Generally the crustal rocks do not melt at this temperature. Therefore the presence of fluids is more likely to increase the conductivity of the lower crust.

Some discussion are available in the literature on the possible existence of graphite at lower crustal depth (Haak and Hutton, 1986; Duba and Shankland, 1982; Shankland and Anders, 1983, Fyfe, 1988). Mareschal et

al. (1992) have proved the existence of grain boundary graphite in Kapuskasing uplift, which can enhance the lower crustal conductivity. Field work in the array form and 3-D MT modelling in future will throw further light on the possible existence and geometry of these lower crustal conductors (Park, 1985; Ranganayaki and Madden, 1980)

Acknowledgement

Authors are grateful to the Department of Science and Technology, New Delhi for sanctioning the projects SP/S2/P20A/85 and ESS/CA/A8-02/89. Authors are grateful to Mr. A. Chattopadhyay for participating in the field program and collecting field data. Authors are grateful to Prof. John Booker for providing the INV2D program. Thanks are due to Mr. P.K. Hazra for drafting the diagrams neatly.

References

Anderson, D.L. (1995). Lithosphere, Asthenosphere and Perisphere. *Rev. Geophy.*, **33**(1), 125–149.

Bachus, G.E. and Gilbert, F. (1968). The resolving power of gross earth data. *Geophy. Jour. R. Astro. Soc.*, **16**, 169–205.

Bachus, G.E. and Gilbert, F. (1970). Uniqueness in the inversion of inaccurate gross earth data. *Philosophical. Trans. R. Soc. London*, **266**, 123–192.

Bakshi, A.K., Archibald, D.A., Sarkar, S.N., and Saha, A.K. (1987). 40Ar–39Ar increment heatup study for mineral separates from the Early Archaean east India craton: implication of a thermal history of a section of the batholith complex. *Can. Jour. Earth Science*, **24**, 1985–1997.

Banerjee, P.K. and Ghosh, S. (1994). Is the Simlipal Complex a product of shallow plume tectonics. *Jour. Geol. Soc. India,* **43**, 353–359.

Bradley, R.S., Jamil, A.K., and Munro, D.C. (1964). The electrical conductivity of olivine at high temperatures and pressures. *Geochimica Cosmochimica Acta,* **28**, 1669–1678.

Chanishvilli, Z.V., Lastovickova, M., and Kropacek, V. (1982). Thermal and electric conductivity of three basaltic rocks of the Bohemian Massif under high temperatures. *Studia Geophy. et Geodaet.*, 26, 93–95.

Constable, S. and Duba, A. (1990). Electrical a conductivity of olivine, a denote and the mantle. *Jour. Geophy. Res;* **95**, 6967–6978.

Constable, S., Shankland, T.J., and Duba, A.G. (1992). The electrical conductivity of an isotropic olivine mantle. *Jour. Gephy. Res.*, **97**(B3), 3397–3404.

Duba, A.G. (1976). are laboratory electrical conductivity data relevant to the Earth? *Acta Geod. Geoph. Mont., Hungary,* **11**, 485–495.

Duba, A.G. and Nicholls, I.A. (1973). The influence of oxidation state on the electrical conductivity of olivine. *Earth and Planet. Sci. Lets.*, **18**, 59–64.

Duba, A.G. and Shankland, T.J. (1982). Free carbon and electrical conductivity in the earth's mantle. *Geophy. Res. Let.*, **9**(11), 1271–1275.

Duba, A., Baland, J.N., and Ringwood, A.E. (1973). The electrical conductivity of pyroxene. *Jour. of Geology,* **81**, 727–735.

Duba, A., Heard, H.C., and Schock, R.N. (1974). Electrical conductivity of olivine at high pressure and under controlled oxygen fugacity. *Jour. Geophy. Res.*, **79**, 1667–1673.

Dvorak, Z. (1973). Electrical conductivity of several samples of olivenites, peridotites and dunites as a function of pressure and temperature. *Geophysics,* **38**, 14–24.

Eggers, D.W. (1982). An eigen state formulation of the MT impedance tensor. *Geophysics,* **47**(8), 1204–1214.

Fyfe, W.S. (1981). Ocean floor hydrothermal activity: The oceanic lithosphere. In Emiliani, C., ed., *The Sea,* volume 7, pp. 589–638. John Wiley & Sons, New York.

Fyfe, W.S. (1986). Fluids in deep continental crust. *Jour. Geophy. Res.*

Fyfe, W.S. (1988). Granites and a wet convecting ultramafic planet. *Trans. R. Soc. Edinburgh, Earth Sciences,* **79,** 339–346.

Gokarn, S.G., Rao, C.K., Singh, B.P., and Nayak, P.N. (1992). Magnetotelluric studies across the Kurduwadi gravity features. *Phys. Earth Planet. Inter.*, **72**, 58–67.

Haak, V. and Hutton, R. (1986). The nature of lower continental crust. *Geolgical society special publication,* **24**, 35–49.

Hoerl, A.E. and Kennard, R.W. (1970)a. Ridge regression, application to non orthogonal problem. *Tectonometrics*, **12**, 69–82.

Hoerl, A.E. and Kennard, R.W. (1970)b. Ridge regression; baised estimation for non orthogonal problem. *Tectonometrics,* **12**, 55–67.

Hyndeman, R.D. and Hyndeman, D.W. (1968). Water saturation and higher electrical conductivity in the lower continental crust. *Earth and Planet. Sci. Lets.*, **4,** 427–432.

Hyndeman, R.D. and Shearer, P.M. (1989). Water in the lower continental crust: modelling magnetotelluric and seismic reflection results. *Geophy. Jour. R. Astro. Soc.*, **98**, 343–365.

Inman, J.R. (1975). Resistivity inversion with ridge regression. *Geophysics,* **40**, 798–817.

Jones, A.G. (1988). Static shift of magnetotelluric data and its removal in a sedimentary basin environment. *Geophysics,* **53**, 967–978.

Kariya, K.A. and Shankland, T.J. (1983). Electrical conductivity of dry lower crustal rocks. *Geophysics*, **48**, 52–61.

Kirkpatrik, S., Gelatt, C.D., and Vecchi, M.P. (1983). Optimisation by simulated annealing. *Science*, **220**, 4598.

Kobayashi, Y. and Maruyama, H. (1971). Electrical conductivity of olivine, single crystals at high temperatures. *Earth and Planet. Sci. Lets.*, **11**, 415–419.

Lastovickova, M. (1975). The electrical conductivity of eclogites measured by two methods. *Studia Geophy. et Geodaet.*, **19**, 394–398.

Lastovickova, M. (1979). Electrical conductivity of Teschenites Trachy andesites and Basalts under high temperatures. *TravauX De L' institut Geophysique de L' Academic TchecosLovaque Des Sciences,* **529**, 233–250.

Lastovickova, M. (1983). Electrical conductivity of garnets and garnet bearing rockes. *Gerlands Beitrage zur Geophysik;* **90.6**, 529–536.

Lastovickova, M. (1981). Laboratory measurements of electrical properties of rocks and minerals. *Geophy. Surv.*, **6**, 201–213.

Lastovickova, M. and Kropacek, V. (1978). Changes of electrical conductivity in the neighbourhood of the Curie temperature of basalts. *Studia Geophy. et Geodaet.*, **20**, 265–271.

Lastovickova, M., Ramana, Y.S., and Gogte, B.S. (1987). Electrical conductivity of some rocks from the Indian subcontinents. *Studia Geophy. et Geodaet.*, **31**, 60–72.

Mackwell, S.J. and Kohlstedt, D.L. (1990). Diffusion of hydrogen in olivine: implications for water in the mantle. *Jour. Geophy. Res.*, **95**, 5079–5088.

Mareschal, M., Fyfe, W.S., Percival, J., and Chan, T. (1992). Grain-boundary graphite in Kapuskasing gneisses and implications for lower crustal conductivity. *Nature,* **357**, 674–676.

Marquardt, D.W. (1963). An algorithm for least square estimation of nonlinear parameters. *Jour. Soc. Ind. App. Math.*, **2,** 431–441.

Nixon, P.H. (1987). *Mantle Xenoliths.* John wiley and Sons, New York.

Olhoeft, G.R. (1977). Electrical properties of water saturated basalt: Preliminary results to 506 K (233°C). Technical Report D-77–688, USGS open file Report.

Omura, K., Kurita, K., and Kamazawa, M. (1989). Experimental study of pressure dependence of electrical conductivity at high temperatures. *Phys. Earth Planet. Inter.,* **57**, 291–303.

Park, S.K. (1983). *Three dimensional magnetotelluric modelling and inversion.* PhD thesis, Mass. Inst. Tech., Cambridge, Massachusetts.

Park, S.K. (1985). Distortions of magnetotelluric sounding curves by three dimensional structures. *Geophysics,* **50**(5), 785–797.

Pollack, H.N. and Chapman, D.S. (1977). On the regional variation of heat flow, geotherm and lithosphere thickness. *Tectonophysics*, **38**, 279–296.

Rai, C.S. and Manghnani, M.H. (1978). Electrical conductivity of ultramafic rocks to 1820°C Kelvin. *Phys. Earth Planet. Inter.,* **17**, 6–13.

Ranganayaki, R.P. and Madden, T.R. (1980). Generalised thin sheet analysis in magnetotelluric: an extension of Price's analysis. *Geophy. Jour. R. Astro. Soc.,* **60**, 445–457.

Roy, K.K. (1996). Electrical charaterisation of some parts of the Singhbhum Orissa Iron Ore Craton. Project Report, No. ESS/CA/A8-02/89.

Roy, K.K. and Routh, P.S. (1994). Nonlinear resistivity inversion using Simulated Annealing, an example for Singhbhum Orissa iron ore craton. *Ind. Jour. Earth Sci.,* **21,** 209–218.

Roy, K.K., Mukherjee, K.K., Singh, A.K., and Das, L.K. (1993). Geophysical evidence for existence of two distinct bodies of granite in the central part of the Singhbhum granite batholith, Eastern India. *Ind. Jour. Earth Sci.,* **20**(3–4), 142–152.

Saha, A.K. (1994). Crustal evolution of Singhbhum—North orissa, Eastern India. *Memoirs of Geol. Soc. India,* **27**.

Saha, A.K., Sankaran, A.V. and Bhattacharyya, T.K. (1968). Trace element distribution in the magmatic and metasomatic granites of Singhbhum region, Eastern India, Neves. Jahrb. Min. Abh. **108**, 247–270.

Saha, A.K., Ghosh, S., Dasgupta, S., Mukhopadhyay, and Roy, S.L. (1984). Studies on crustal evolution of the Singhbhum Orissa Iron Ore Craton, Monograph on crustal evolution. *Ind. Soc. Earth Sci.,* **SPL**., 1–74.

Saha, A.K., Ray, S.L., and Sarkar, S.N. (1988). Early history of the earth; evidence from the eastern Indian Shield in Precambrian of the Eastern Indian shield. *Jour. Geol. Soc. India,* **8**, 13–38.

Schock, R.N., Duba, A.G., and Shankland, T.J. (1989). Electrical conduction in Olivine. *Jour. Geophy. Res.,* **94**(B5), 5829–5839.

Sen, M.K. and Stoffa, P.L. (1991). Nonlinear one dimensional seismic waveform inversion using simulated annealing. *Geophysics*, **56**, 1624–1638.

Shankar, R. (1988). Heat flow map of India and discussion on its geological and economic significance. *Indian Minerals,* **42**(2), 89–110.

Shankland, T.J. and Anders, M.E. (1983). Electrical conductivity, Temperature and fluids in the lower crust. *Jour. Geophy. Res.,* **88**(11.3), 9475–9484.

Shankland, T.J. and Duba, A.G. (1987). Spatially averaged electrical conductivity curve for olivine. *EOS, Trans. Am. Geophy. Union,* **68**, 1503.

Shankland, T.J. and Duba, A.G. (1990). Standard electrical conductivity of isotropic homogeneous olivine in the temperature range 1200–1500°C. *Geophy. Jour. Internat.,* **103,** 25–31.

Smith, J.T. and Booker, J.R. (1991). Rapid inversion of two and three dimensional magnetotelluric data. *Jour. Geophy. Res.,* **96**, 3905–3922.

Swift, C.M. (1969). *A magnetotelluric investigation of an electrical conductivity anomaly in the South Western United States.* PhD thesis, Massachusetts Institute of Technology, Cambridge, MA.

Tyburczy, J.A. and Roberts, J.J. (1990). Low frequency electrical response of polycrystalline olivine compacts: Grain boundary transport. *Geophy. Res. Let.*, **17**, 1985–1988.

Verma, R.K. and Mukhopadhyay, M. (1989). Gravity survey of the Singhbhum Orissa iron ore craton. Report No. DST SP/S2/P20B/85.

Vozoff, K. (1972). The magnetotelluric method in the exploration of sedimentary basins. *Geophysics*, **37**(1), 91–141.

Wyllie, P.J. (1988). Magma genesis, plate tectonics and chemical differentiation of the earth. *Rev. Geophy.*, **36**(3), 370–404.